AIAA JOURNAL
Vol. 43, No. 9, September 2005

Mean-Flow-Multigrid for Implicit Reynolds-Stress-Model Computations

G. A. Gerolymos* and I. Vallet†
Université Pierre-et-Marie-Curie, 75252 Paris Cedex 05, France

The purpose of this work is to develop an efficient and robust multigrid acceleration technique for the computation of the compressible Favre–Reynolds-averaged Navier–Stokes equations with seven-equation Reynolds-stress-model turbulence closures. The basic monogrid algorithm uses an upwind-biased $\mathcal{O}(\Delta x^3)$ flux-vector-split space discretization with implicit time integration. The discrete system of nonlinear equations is solved by a subiterative procedure, based on a local dual-time-stepping technique, which includes quasi-Newton iteration in the limit $\Delta t \rightarrow \infty$. Full-approximation scheme sawtooth cycle multigrid is applied on the mean-flow variables only, while turbulence variables are simply injected into coarser grids. Characteristic-based multigrid is used for the restriction operator. The straightforward extension of the method to lower-level two-equation k–ε closures is described. Computational examples for various two- and three-dimensional complex flows, including large separation and/or shock-wave/boundary-layer interactions using different turbulence models, demonstrate that speed-ups of 3 to 4 are obtained, using three levels of multigrid (fine + two coarser grids).

Introduction

WORK on the careful implementation of full Reynolds-stress model[1] (RSM) seven-equation turbulence closures has contributed to the development of efficient and robust computational methods for complex compressible flows.[2–13] All of these methods are upwind (or upwind biased) and implicit[14] to achieve the desirable robustness and efficiency. Multigrid[15] convergence acceleration is expected to further enhance computational efficiency.

There is, however, very little published work on multigrid solvers by using full seven-equation turbulence closures. Demuren[16] computed quasi-incompressible flow of multiple three-dimensional turbulent jets in a crossflow, using an implicit pressure-based[14] algorithm, and a full-approximation scheme/full-multigrid[15] (FAS-FMG) technique. The multigrid algorithm was applied on the mean-flow variables only. The Reynolds-stress-transport equations were solved on the fine grid only, and the Reynolds stresses were simply injected into the coarser grids. Lien and Leschziner[17] computed incompressible flow over a backward-facing step, also using a pressure-based[14] method, and a FAS technique,[15] and applied multigrid to the turbulence variables also, introducing three stabilizing measures: 1) the source terms for the turbulence equations were computed on the fine grid and restricted onto coarser grids, 2) the coarse-grid corrections for the turbulence variables were underrelaxed prior to prolongation, and 3) the prolongation operator is conditioned to ensure positivity, for the variables that must remain positive (k, ε, $\overline{u'u'}$, $\overline{v'v'}$, $\overline{w'w'}$), by splitting the coarse-grid corrections into negative and positive parts [e.g., for the turbulence-kinetic energy $\Delta k \leftarrow \Delta k(\Delta k + \Delta k^+)/(\Delta k - \Delta k^-)$, where Δk, Δk^+, Δk^- are the corrections and their positive and negative parts respectively].

The bulk of the published work on multigrid solvers for the Favre–Reynolds-averaged Navier–Stokes equations with transport equations near-wall turbulence closures is concerned with one- or two-equation closures.[18–26] A review of this work indicates that the multigrid treatment of the source terms is of major concern,[18–26] contrary to monogrid methods.[10,13,27] The associated problems can be traced to the fact that the mean-flow (MF) velocity gradients appearing in the source terms are not satisfactorily computed on the coarse grids, and this can induce substantial convergence problems.[22,23,26] The usual solution is to compute the mean-flow velocity gradients appearing in the source terms or in their Jacobians on the fine grid only and to restrict them onto coarser grids.[18,22,23,26] These stabilizing measures appear to be independent of the particular turbulence closure variant[1,28,29] used.

Gerolymos[18] computed several transonic shock-wave/turbulent-boundary-layer interactions, with a k–ε model,[28] using the multiple-grid algorithm of Ni[30] (based on the centered Lax–Wendroff scheme with implicit residual smoothing[14]). The multiple-grid algorithm of Ni[30] is not a FAS multigrid,[15] but uses instead second-order changes to propagate residuals on the coarser grids [in the same way that the Lax–Wendroff scheme uses second time derivatives to obtain $\mathcal{O}(\Delta t^2)$ accuracy[14]]. As a consequence, the Jacobians of the fluxes $(\partial \underline{F}_\ell/\partial \underline{w})$ and of the source terms $(\partial \underline{S}/\partial \underline{w})$ are computed on the fine grid only and then restricted onto coarser grids (volume-weighted averaging was used as the restriction operator).

Sikonen[19] computed two- and three-dimensional flows past airfoils and wings, with a k–ε model,[28] using an implicit upwind scheme.[14] Sikonen[19] applied FAS multigrid,[31] where 1) the turbulent viscosity was computed only on the finest grid and injected into coarser grids and 2) the increments of k and ε were strongly underrelaxed in the prolongation phase.

Liu and Zheng[20] computed steady and unsteady[32] (by using dual time stepping[33–36]) flows past airfoils and cascades, with a k–ω_T model,[29] using a centered scheme with implicit residual smoothing,[37] and a staggered finite volume discretization for the k–ω_T model.[38] A FAS multigrid[39] algorithm was used, and the k–ω_T equations were stabilized by computing the mean-flow velocity gradients appearing in the source terms on the finest grid only and restricting them onto coarser grids. Park and Kwon[40] adapted the method of Liu and Zheng[20] to an implicit time integration and applied it to flow around airfoils.

Dick and Steelant[21] computed zero-pressure-gradient turbulent boundary layers, using various k–ε models,[28] and several implicit upwind methods,[41] with a FAS multigrid algorithm. The k–ε computations were stabilized by using a procedure similar to Lien and Leschziner,[17] combining underrelaxation and positivity constraints in the prolongation phase of coarse-grid corrections $[\Delta k \leftarrow \Delta k(\Delta k + \alpha \Delta k^+)/(\Delta k - \alpha \Delta k^-);\ \alpha = 0.3]$.

Presented as Paper 2004-2527 at the AIAA 34th Fluid Dynamics Conference, Portland, OR, 28 June–1 July 2004; received 7 October 2004; revision received 25 January 2005; accepted for publication 3 February 2005.

*Professor, Director, Laboratoire d'Energétique, Case 800, 4 place Jussieu; geg@ccr.jussieu.fr. Member AIAA.

†Assistant Professor, Laboratoire d'Energétique, Case 800, 4 place Jussieu; vallet@ccr.jussieu.fr. Member AIAA.

Gerlinger and Brüggemann[22] computed several supersonic flows,[22,23,25] by using a $\sqrt{k}-\omega_T$ model,[42] with a centered implicit scheme,[31] and a FAS multigrid algorithm.[31] Again, the mean-flow gradients appearing in the source terms of the turbulence transport equations were computed on the finest grid only and then restricted onto coarser grids by volume-weighted averaging.

Lambropoulos et al.[26] computed transonic two- and three-dimensional flows past cascades, airfoils and wings, by using a k–ε model[28] and an upwind implicit scheme on unstructured grids, with FAS agglomeration multigrid.[43] The k–ε equations were stabilized by 1) computing mean-flow velocity gradients on the fine grid only and restricting them by volume-weighted averaging, 2) restricting only positive residuals of the turbulence variables onto coarser grids, and 3) prolongating only positive corrections of the turbulence variables on the fine grid.

Similar procedures are used by various authors applying multigrid on one-equation closures.[24,26]

The preceding remarks apply to nonlinear multigrid methods.[44] Linear multigrid, aiming at accelerating the linear system solution at each iteration by iterative unfactored methods,[44] does not require reevaluation of residuals on coarser grids. Carré[45] and Carré et al.[46] has computed transonic flows around airfoils, by using a k–ε model,[28] and an upwind implicit scheme on unstructured grids, applying linear agglomeration multigrid,[43] without any particular treatment.

Obviously a multigrid procedure applied to the Reynolds-stress-transport equations should 1) evaluate source terms by using mean-flow velocity gradients computed on the fine grid and restricted onto coarser grids and 2) include some procedure limiting restriction of residuals and/or prolongation of coarse-grid corrections so as to satisfy positivity of ε and realizability of the Reynolds-stress tensor.[47] This is the subject of ongoing research.

In the present work, this problem is avoided by using a full-approximation-scheme (FAS) multigrid method for the mean-flow variables only. Turbulence variables (Reynolds stresses and dissipation) are updated only on the fine grid and are simply injected into coarser grids. Several authors[16,48–50] have applied this technique and have in general obtained satisfactory speed-ups. Although it is possible that this approach can lead to saturation of residuals,[24] it offers several advantages:

1) It avoids redeveloping source treatment approaches when using the computational method for turbulence model development purposes; in this context, source terms, especially redistribution terms, are modified between variants,[51,52] taking into account the fact that the derivatives of source terms have quite lengthy expressions for three-dimensional Reynolds-stress closures,[53] recoding them for each variant can be very time consuming.

2) It avoids storage of source terms or associated gradients on the fine grid, for use in the restriction phase, which can result in substantial increase of computer-memory requirements, especially when using fine multiblock meshes for geometrically complex applications.[54]

3) It can be used with any turbulence closure, either one-, two-, or seven-equation (RSM), without modification, provided that the appropriate turbulence variables are injected into the coarser grids.

The underlying idea is that turbulence reacts very rapidly to MF variations through the source terms. (In a full RSM closure context the production and rapid redistribution terms are the most important.[52]) Acceleration of the MF variables also accelerates the convergence of turbulence variables through the source terms (which depend on MF gradients).

The present paper describes the development of mean-flow-multigrid methods used for convergence acceleration of a baseline implicit solver of the Navier–Stokes equations with near-wall RSM seven-equation closure.[13] (Both the baseline and the multigrid algorithms can also be used for lower-level one- or two-equation closures.) To the authors' knowledge, there has been no other attempt to apply multigrid acceleration techniques for the compressible three-dimensional Navier–Stokes equations with RSM closure. (The work of Lien and Leschziner[17] and of Demuren[16] concerned incompressible flows.) After a brief description of the flow model and of the baseline monogrid scheme,[13] a FAS-multigrid technique, in which the mean-flow part of the baseline scheme is applied on each successively coarser grid, is developed. The method is evaluated in two-dimensional computations of oblique shock-wave/turbulent-boundary-layer separated-flow interaction at a $M_{SW}\sim 3$ compression ramp,[55,56] for various turbulence models, both two-equation[28] and RSM.[52] A multiblock extension of the method, using phantom nodes to transfer information between grid domains,[57] is then applied to the computation of a high-subsonic (inflow Mach number $M_i\sim 0.6$) annular cascade, with large hub corner stall.[58,59]

Flow Model and Monogrid Flow Solver

Flow Model

The flow is modeled by the compressible Favre–Reynolds-averaged three-dimensional Navier–Stokes equations,[51] coupled to the six transport equations for the Reynolds stresses and the transport equation for the turbulence-kinetic-energy modified dissipation rate,[51] written symbolically as

$$\frac{\partial \underline{w}}{\partial t}+\frac{\partial \underline{F}_\ell}{\partial x_\ell}+\underline{S}\equiv \frac{\partial \underline{w}}{\partial t}+\frac{\partial \underline{F}_x}{\partial x}+\frac{\partial \underline{F}_y}{\partial y}+\frac{\partial \underline{F}_z}{\partial z}+\underline{S}=0 \qquad (1)$$

where

$$\underline{w}=\left[\underline{w}_{\mathrm{MF}}^T,\underline{w}_{\mathrm{RSM}}^T\right]^T=\left[[\bar\rho,\bar\rho\tilde u,\bar\rho\tilde v,\bar\rho\tilde w,\bar\rho\check h_t-\bar p];\right.$$
$$\left.[\bar\rho\widetilde{u''u''},\bar\rho\widetilde{u''v''},\bar\rho\widetilde{v''v''},\bar\rho\widetilde{v''w''},\bar\rho\widetilde{w''w''},\bar\rho\widetilde{w''u''},\bar\rho\varepsilon^*]\right]^T\in\mathbb{R}^{12} \qquad (2)$$

is the vector of unknowns, $\underline{w}_{\mathrm{MF}}\in\mathbb{R}^5$ is the vector of mean-flow variables, $\underline{w}_{\mathrm{RSM}}\in\mathbb{R}^7$ is the vector of turbulence variables (Reynolds stresses and dissipation rate), $\underline{F}_\ell\in\mathbb{R}^{12}$ ($\underline{F}_x,\underline{F}_y,\underline{F}_z$) are the combined convective ($\underline{F}_\ell^C$) and diffusive (viscous; $\underline{F}_\ell^V$) fluxes ($\underline{F}_\ell=\underline{F}_\ell^C+\underline{F}_\ell^V$), $\underline{S}\in\mathbb{R}^{12}$ are the source terms, t is the time, x_ℓ (x,y,z) are the Cartesian space coordinates, u_ℓ (u,v,w) are the velocity components, ρ is the density, p is the pressure, $\tilde h_t=\tilde h+\frac{1}{2}\tilde u_i\tilde u_i$ is the total enthalpy of the mean flow, h is the specific enthalpy, and ε^* is the modified[28] dissipation rate ($\varepsilon^*=\varepsilon-2\check\nu[\mathrm{grad}(\sqrt{k})]^2$), ε is the dissipation rate, $k=\frac{1}{2}u_i''u_i''$ is the turbulence kinetic energy, and ν is the kinematic viscosity. The symbol ($\tilde{}$) indicates Favre averaging, ($\bar{}$) nonweighted averaging, ($''$) Favre fluctuations, and ($'$) nonweighted fluctuations. The symbol ($\check{}$) is used to denote a function of average quantities that is neither a Favre average nor a nonweighted average. The exact expressions of the fluxes $\underline{F}_\ell$ and the source terms $\underline{S}$ depend on the particular model used and are given in the corresponding references.[10,13,51,52] The numerical method presented is designed to be relatively independent of the particular RSM closure used and is also applicable to two-equation closures, as described in the Application to Two-Equation Closures section. The monogrid scheme has been described in detail by Chassaing et al.,[13] and only some basic elements, necessary for the description of the multigrid methods developed in the present work, are given in the following.

Discretization

These equations (1) are discretized on a structured grid using a finite volume technique with vertex storage.[60] The divergence of convective fluxes ($[\underline{F}_x^C,\underline{F}_y^C,\underline{F}_z^C]^T\in\mathbb{R}^{12}\otimes\mathbb{E}^3$) is discretized using the flux-vector-splitting method of Van Leer with $\mathcal{O}(\Delta x^3)$ monotone upstream-centered scheme for conservation laws (MUSCL) interpolation and Van Albada limiters.[61,62] The divergence of viscous fluxes ($[\underline{F}_x^V,\underline{F}_y^V,\underline{F}_z^V]^T\in\mathbb{R}^{12}\otimes\mathbb{E}^3$) is discretized using an $\mathcal{O}(\Delta x^2)$ stencil.[63] Noting (ξ,η,ζ) the grid directions (i,j,k), $({}^\xi\mathcal{S}_{i\pm1/2,j,k},{}^\eta\mathcal{S}_{i,j\pm1/2,k},{}^\zeta\mathcal{S}_{i,j,k\pm1/2})$ the cell-face areas of the staggered grid cell around the point (i,j,k), and

$$\left(\left[{}^\xi n_x,{}^\xi n_y,{}^\xi n_z\right]^T_{i\pm\frac12,j,k},\left[{}^\eta n_x,{}^\eta n_y,{}^\eta n_z\right]^T_{i,j\pm\frac12,k},\right.$$
$$\left.\left[{}^\zeta n_x,{}^\zeta n_y,{}^\zeta n_z\right]^T_{i,j,k\pm\frac12}\right)$$

the corresponding unit normals (positive in the positive grid direction), the semidiscrete scheme can be written[13]

$$\frac{\mathrm{d}\underline{w}_{i,j,k}}{\mathrm{d}t} + \underline{\mathcal{L}}_{i,j,k} \equiv \frac{\mathrm{d}\underline{w}_{i,j,k}}{\mathrm{d}t} + \frac{1}{\mathcal{V}_{i,j,k}} \begin{bmatrix} +^{\xi}\mathcal{S}_{i+\frac{1}{2},j,k}\ {}^{\xi}\underline{F}^{N}_{i+\frac{1}{2},j,k} - {}^{\xi}\mathcal{S}_{i-\frac{1}{2},j,k}\ {}^{\xi}\underline{F}^{N}_{i-\frac{1}{2},j,k} \\ +^{\eta}\mathcal{S}_{i,j+\frac{1}{2},k}\ {}^{\eta}\underline{F}^{N}_{i,j+\frac{1}{2},k} - {}^{\eta}\mathcal{S}_{i,j-\frac{1}{2},k}\ {}^{\eta}\underline{F}^{N}_{i,j-\frac{1}{2},k} \\ +^{\zeta}\mathcal{S}_{i,j,k+\frac{1}{2}}\ {}^{\zeta}\underline{F}^{N}_{i,j,k+\frac{1}{2}} - {}^{\zeta}\mathcal{S}_{i,j,k-\frac{1}{2}}\ {}^{\zeta}\underline{F}^{N}_{i,j,k-\frac{1}{2}} \end{bmatrix} + \underline{S}_{i,j,k} \cong 0 \qquad \forall i, j, k \tag{3}$$

where $\mathcal{V}_{i,j,k}$ is the control volume, $\underline{F}^N$ denotes the numerical fluxes, and $\underline{\mathcal{L}}_{i,j,k}$ is the discretized form of the space operator [divergence and source terms; Eq. (3)]. Full details for the discretization are given in Chassaing et al.[13,36] For steady flows, an $\mathcal{O}(\Delta t)$ backward-Euler fully implicit scheme is used, which at iteration level n reads[13,36,61,62]

$$\frac{{}^{n+1}\underline{w}_{i,j,k} - {}^{n}\underline{w}_{i,j,k}}{\Delta t_{i,j,k}} + {}^{n+1}\underline{\mathcal{L}}_{i,j,k} \cong 0 \quad \forall\ i, j, k \Longleftrightarrow \frac{{}^{n+1}\mathfrak{w} - {}^{n}\mathfrak{w}}{\Delta \mathfrak{t}} + \mathfrak{L}({}^{n+1}\mathfrak{w}) \cong 0 \tag{4}$$

where

$$\mathfrak{w} = \left[\underline{w}^T_{1,1,1}, \underline{w}^T_{1,1,2} \ldots, \underline{w}^T_{N_i,N_j,N_k}\right]^T \in \mathbb{R}^{12\times N_i \times N_j \times N_k}$$

and

$$\mathfrak{L} = \left[\underline{\mathcal{L}}^T_{1,1,1}, \underline{\mathcal{L}}^T_{1,1,2}, \ldots, \underline{\mathcal{L}}^T_{N_i,N_j,N_k}\right]^T \in \mathbb{R}^{12\times N_i \times N_j \times N_k}$$

are the global vectors of the unknowns and of the space operators, respectively, and $\Delta \mathfrak{t} = \mathrm{diag}[(\Delta t_{1,1,1})\underline{\underline{I}}_{12}, (\Delta t_{1,1,2})\underline{\underline{I}}_{12}, \ldots, (\Delta t_{N_i,N_j,N_k})\underline{\underline{I}}_{12}]$ (where $\underline{\underline{I}}_{12}$ denotes the 12×12 identity matrix and $1/\Delta \mathfrak{t} \equiv \Delta \mathfrak{t}^{-1}$).

Subiterative Solution of the Nonlinear System

Local Dual Time Stepping

The nonlinear system obtained from the preceding discretization [Eqs. (4)] for the global vector of unknowns $\mathfrak{w}$ is solved using a subiterative approach, based on a local-dual-time-stepping (LDTS) procedure,[13] inspired from the corresponding dual-time-stepping (DTS) approach, which is widely used for time-consistent unsteady flow computations.[33–36] Note that Zhao[64] has recently used a DTS technique for the computation of steady flow with a low-turbulence Reynolds-number two-equation closure. Introducing a pseudo time step, $\Delta t^*_{i,j,k}$, and the associated diagonal matrix $\Delta \mathfrak{t}^* = \mathrm{diag}[(\Delta t^*_{1,1,1})\underline{\underline{I}}_{12}, (\Delta t^*_{1,1,2})\underline{\underline{I}}_{12}, \ldots, (\Delta t^*_{N_i,N_j,N_k})\underline{\underline{I}}_{12}]$, the local dual-time-stepping procedure pseudo-time marched (subiteration counter $m_{\mathrm{it}} \equiv m$; pseudo time step Δt^*) the nonlinear system [Eqs. (4)] at each iteration (iterations counter $n_{\mathrm{it}} \equiv n$; time step Δt)

$$\frac{{}^{m+1,n+1}\mathfrak{w} - {}^{m,n+1}\mathfrak{w}}{\Delta \mathfrak{t}^*} + \frac{{}^{m+1,n+1}\mathfrak{w} - {}^{n}\mathfrak{w}}{\Delta \mathfrak{t}} + \mathfrak{L}({}^{m+1,n+1}\mathfrak{w}) \cong 0 \tag{5}$$

which is linearized, by Taylor-expanding $\mathfrak{L}({}^{m+1,n+1}\mathfrak{w})$, as

$$\frac{{}^{m+1,n+1}\mathfrak{w} - {}^{m,n+1}\mathfrak{w}}{\Delta \mathfrak{t}^*} + \frac{{}^{m+1,n+1}\mathfrak{w} - {}^{n}\mathfrak{w}}{\Delta \mathfrak{t}} + \mathfrak{L}({}^{m,n+1}\mathfrak{w}) + \frac{\partial \mathfrak{L}^J}{\partial \mathfrak{w}}({}^{m,n+1}\mathfrak{w})[{}^{m+1,n+1}\mathfrak{w} - {}^{m,n+1}\mathfrak{w}] \cong 0 \tag{6}$$

and solved for ${}^{m+1,n+1}\mathfrak{w} - {}^{m,n+1}\mathfrak{w}$

$$\left[\mathfrak{I} + \Delta \mathfrak{t}^{**}\frac{\partial \mathfrak{L}^J}{\partial \mathfrak{w}}({}^{m,n+1}\mathfrak{w})\right][{}^{m+1,n+1}\mathfrak{w} - {}^{m,n+1}\mathfrak{w}] \cong -\Delta \mathfrak{t}^{**}\left[\frac{{}^{m,n+1}\mathfrak{w} - {}^{n}\mathfrak{w}}{\Delta \mathfrak{t}} + \mathfrak{L}({}^{m,n+1}\mathfrak{w})\right] = -\Delta \mathfrak{t}^{**}[\mathfrak{R}({}^{m,n+1}\mathfrak{w}, {}^{n}\mathfrak{w}, \Delta \mathfrak{t})] \tag{7}$$

where $\mathfrak{I} \in \mathbb{R}^{(12\times N_i \times N_j \times N_k)\times(12\times N_i \times N_j \times N_k)}$ is the identity matrix, $\mathfrak{R}({}^{m,n+1}\mathfrak{w}, {}^{n}\mathfrak{w}, \Delta \mathfrak{t}) = [{}^{m,n+1}\mathfrak{w} - {}^{n}\mathfrak{w}]/\Delta \mathfrak{t} + \mathfrak{L}({}^{m,n+1}\mathfrak{w})$ is the residual with space operator computed at ${}^{m,n+1}\mathfrak{w}$ and time derivative evaluated between ${}^{m,n+1}\mathfrak{w}$ and ${}^{n}\mathfrak{w}$ with time step $\Delta \mathfrak{t}$, ${}^{1,n+1}\mathfrak{w} = {}^{n}\mathfrak{w}$ is the initial value for the subiterations, and $\Delta \mathfrak{t}^{**} = [\mathfrak{I} + \Delta \mathfrak{t}^{-1}\Delta \mathfrak{t}^*]^{-1}\Delta \mathfrak{t}^*$. The Jacobian matrix $\partial \mathfrak{L}^J/\partial \mathfrak{w}$ is an approximation to the exact Jacobian $\partial \mathfrak{L}/\partial \mathfrak{w}$, chosen so as to minimize implicit work for the turbulence variables.[13] To ensure stability at high time steps ($\Delta \mathfrak{t}^*$), implicit boundary conditions are applied following the method of characteristics approach of Chakravarthy,[65] which implies appropriate modifications of the Jacobians $\partial \mathfrak{L}^J/\partial \mathfrak{w}$ and of the residue $\mathfrak{R}$ to conform with boundary conditions.[53]

Boundary Conditions and Realizability Constraints

At each subiteration [Eqs. (6)] boundary conditions are applied not only implicitly but also explicitly. This is useful not only because the linear system [Eq. (7)] is only solved approximately, but also because in some instances boundary conditions can be nonlocal.[66] The explicit application of boundary conditions will be represented by the operator $\boldsymbol{B}(\mathfrak{w})$.

It is quite possible, during the iterations, to obtain Reynolds stresses that do not satisfy the realizability constraints introduced by Schumann.[47] Such anomalous behavior is systematically checked for at every subiteration. If the realizability constraints are not satisfied for a given grid point, then all turbulence variables are set to zero at this grid point:

$$\text{if} \left\{ \begin{array}{ccc} \widetilde{u''^2} < 0 \vee & \widetilde{v''^2} < 0 \vee & \widetilde{w''^2} < 0 \vee \\ (\widetilde{u''v''})^2 - \widetilde{u''^2}\widetilde{v''^2} > 0 \vee & (\widetilde{v''w''})^2 - \widetilde{v''^2}\widetilde{w''^2} > 0 \vee & (\widetilde{w''u''})^2 - \widetilde{w''^2}\widetilde{u''^2} > 0 \vee \\ \det[\widetilde{u''_i u''_j}] < 0 \vee & \varepsilon^* < 0 \vee & \ell^*_T = k^{\frac{3}{2}}\varepsilon^{*-1} > \ell_{\mathrm{T_{max}}} \end{array} \right\} : \underline{w}_{\mathrm{RSM}} \longleftarrow \underline{0} \tag{8}$$

where $\ell_{\mathrm{T_{max}}}$ is a maximum admissible length scale (a characteristic order-of-magnitude length of the configuration). Divisions by zero are avoided throughout the code by adding 10^{-23} to the denominator [for every fraction $b_1/b_2 \cong b_1/(b_2 + 10^{-23})$]. These simple realizability and boundedness fixes (which are completely explicit and as a consequence easy to implement) were developed in Vallet[53] and were found to stabilize the computations for all of the cases studied using the monogrid method.[13] In subsequent subiterations turbulence builds up again through diffusion from neighboring nodes. These explicit realizability constraints will be represented by the operator $\boldsymbol{R}(\mathfrak{w})$.

Subiterations

The solution of the linear system [Eq. (7)] required at every subiteration m_{it} can be obtained using various methods[67] and in general will be approximate, either because of incomplete convergence of the iterative method used or because of approximate-factorization techniques. Describing the approximate inverse operator by the

subscript APPRX, the $m_{\mathrm{it}} \equiv m$ subiteration reads

$$
\begin{aligned}
{}^{m+1,n+1}\mathfrak{w} &= \boldsymbol{RBR}\left\{ {}^{m,n+1}\mathfrak{w} - \left[\mathfrak{I} + \Delta\mathfrak{t}^{**}\frac{\partial \mathfrak{Q}^J}{\partial \mathfrak{w}}({}^{m,n+1}\mathfrak{w})\right]^{-1}_{\mathrm{APPRX}} \right. \\
&\qquad \left. \times \Delta\mathfrak{t}^{**}[\mathfrak{R}({}^{m,n+1}\mathfrak{w}, {}^{n}\mathfrak{w}, \Delta\mathfrak{t}) + \mathfrak{F}] \right\} \\
&= {}^{m}\boldsymbol{S}({}^{m,n+1}\mathfrak{w}, {}^{n}\mathfrak{w}, \Delta\mathfrak{t}, \Delta\mathfrak{t}^*, \mathfrak{F}) \qquad (9)
\end{aligned}
$$

where $\mathfrak{F} \in \mathbb{R}^{(12 \times N_i \times N_j \times N_k)}$ is a forcing source term, which serves only in the multigrid iteration and which is equal to zero for the monogrid scheme ($\mathfrak{F} = 0$). In the definition of the operator ${}^{m}\boldsymbol{S}({}^{m,n+1}\mathfrak{w}, {}^{n}\mathfrak{w}, \Delta\mathfrak{t}, \Delta\mathfrak{t}^*, \mathfrak{F})$, the variables $[{}^{m,n+1}\mathfrak{w}, {}^{n}\mathfrak{w}]$ indicate the states used to compute the residual $\mathfrak{R}$ [Eq. (7)]. Using the subiteration operator ${}^{m}\boldsymbol{S}$ [Eq. (9)], it is straightforward to write symbolically the full iteration $\boldsymbol{N}(\mathfrak{w}, \mathrm{CFL}, \mathrm{CFL}^*, \mathfrak{F}; M_{\mathrm{it}})$, with a fixed number of subiterations M_{it},

$$
\begin{aligned}
&\{\textbf{do } m_{\mathrm{it}} = 1, M_{\mathrm{it}}, 1; m \equiv m_{\mathrm{it}}; {}^{m+1,n+1}\mathfrak{w} \\
&\quad = {}^{m}\boldsymbol{S}({}^{m,n+1}\mathfrak{w}, {}^{n}\mathfrak{w}, \Delta\mathfrak{t}, \Delta\mathfrak{t}^*, \mathfrak{F}); \textbf{ end do}\} \\
&\quad \Longleftrightarrow {}^{n+1}\mathfrak{w} \equiv {}^{M_{\mathrm{it}}+1,n+1}\mathfrak{w} = \boldsymbol{N}\left({}^{n}\mathfrak{w}, \mathrm{CFL}, \mathrm{CFL}^*, \mathfrak{F}; M_{\mathrm{it}}\right) \qquad (10)
\end{aligned}
$$

or the full iteration $\boldsymbol{N}(\mathfrak{w}, \mathrm{CFL}, \mathrm{CFL}^*, \mathfrak{F}; r_{\mathrm{OBJ}})$ with the number of subiterations fixed dynamically to obtain a given level of error reduction (tolerance) of the increment r_{MF} (Ref. 13):

$$
\begin{aligned}
&\{\textbf{do } m_{\mathrm{it}} \textbf{ while } [r_{\mathrm{MF}} \geq r_{\mathrm{OBJ}}]; m \equiv m_{\mathrm{it}}; {}^{m+1,n+1}\mathfrak{w} \\
&\quad = \boldsymbol{S}({}^{m,n+1}\mathfrak{w}, {}^{n}\mathfrak{w}, \Delta\mathfrak{t}, \Delta\mathfrak{t}^*, \mathfrak{F}); \textbf{ end do}\} \\
&\quad \Longleftrightarrow {}^{n+1}\mathfrak{w} \equiv {}^{r_{\mathrm{OBJ}},n+1}\mathfrak{w} = \boldsymbol{N}\left({}^{n}\mathfrak{w}, \mathrm{CFL}, \mathrm{CFL}^*, \mathfrak{F}; r_{\mathrm{OBJ}}\right) \qquad (11)
\end{aligned}
$$

In both cases [Eqs. (10) and (11)] the subiterations are initialized by ${}^{1,n+1}\mathfrak{w} = {}^{n}\mathfrak{w}$.

There are at this stage two levels of approximation, approximate Jacobians (choice of $\mathfrak{Q}^J$) and approximate inversion {choice of the method of solution of the linear system [Eq. (7)]} which can introduce different variants of the method. The particular approximations used in the present work were those described in Chassaing et al.[13] The method could be further enhanced by using 1) a better approximate factorization technique[67,68] or an unfactored linear system solver[24,41,44] and 2) by including a complete defect correction term in the nonlinear subiteration.[69]

Convergence Monitoring and Time Stepping

The local time step is based on a combined convective (Courant) and viscous [von Neumann (VNN)] criterion[10]

$$
\begin{aligned}
\Delta t_{i,j,k} &= \min\left\{\mathrm{CFL}\left\{\ell_g \Big/ \left[\tilde{V} + \breve{a}\sqrt{1 + \tfrac{5}{6}(\gamma - 1)M_T^2}\right]\right\},\right. \\
&\qquad \left. \mathrm{VNN}\ell_g^2 \Big/ \left(2\nu_{\mathrm{eq}}\right)\right\} \\
\nu_{\mathrm{eq}} &= \max\left\{\tfrac{4}{3}(\breve{\nu} + \nu_T), [(\gamma - 1)/(\bar{\rho}R_g)](\breve{\kappa} + \kappa_T)\right\} \qquad (12)
\end{aligned}
$$

where ℓ_g is the grid-cell size, $\tilde{V}$ is the flow velocity, $\breve{a}$ is the sound velocity, ν_{eq} is the equivalent diffusivity,[70] $\breve{\nu}$ is the molecular kinematic viscosity, $\breve{\kappa}$ is the molecular heat conductivity, $M_T = \sqrt{(2k\,\breve{a}^{-2})}$ is the turbulence Mach number, and the eddy viscosity ν_T and eddy conductivity κ_T are those of the Launder–Sharma k–ε model.[28] This relation [Eq. (12)] is used both for the physical time step ($\Delta t_{i,j,k}$, CFL, VNN) and for the dual pseudo time step ($\Delta t^*_{i,j,k}$, CFL^*, VNN^*).

The parameters controlling the numerical scheme (time integration) are the CFL numbers (CFL for the time step and CFL^* for the dual pseudo time step, assuming that $\mathrm{VNN} = \mathrm{CFL}$ and $\mathrm{VNN}^* = \mathrm{CFL}^*$) and the number of subiterations performed at each iteration $M_{\mathrm{it}}(n_{\mathrm{it}})$. This number can be either fixed by the user [Eqs. (10)], or chosen dynamically based on a convergence criterion for the subiterations [Eqs. (11)]. The relative variation of the mean-flow error e_{MF} is monitored using the following error, L_2, pseudonorm[13]:

$$
\begin{aligned}
e_{\mathrm{MF}}[\mathfrak{w}_{\mathrm{MF}}, \Delta\mathfrak{w}_{\mathrm{MF}}] &= \log_{10} \\
&\times \sqrt{\frac{1}{5}\left\{\frac{\sum[\Delta\bar{\rho}]^2}{\sum[\bar{\rho}]^2} + \frac{\sum[\Delta(\bar{\rho}\tilde{u}_i)\Delta(\bar{\rho}\tilde{u}_i)]}{\sum[\bar{\rho}\tilde{u}_i\bar{\rho}\tilde{u}_i]} + \frac{\sum[\Delta(\bar{\rho}\breve{h}_t - \bar{p})]^2}{\sum[\bar{\rho}\breve{h}_t - \bar{p}]^2}\right\}}
\end{aligned} \qquad (13)
$$

where $\sum$ implies summation over all of the grid nodes, and the summation convention for the Cartesian indices i, $j = 1, 2, 3$ is used. A similar relation[13] is used for the relative variation of turbulence variables e_{RSM}. These quantities e_{MF} and e_{RSM} define approximately the number of digits to which the computation is converged. They are used to define the subiterative convergence of the increment by the error reduction between subiterations $[m, n+1]$ and $[m+1, n+1]$ [Eqs. (9–11)]

$$
\begin{aligned}
r_{\mathrm{MF}}(m+1, n+1) &= \log_{10}\left\{\frac{10^{[e_{\mathrm{MF}}(m+1,n+1)]} - 10^{[e_{\mathrm{MF}}(m,n+1)]}}{10^{[e_{\mathrm{MF}}(m,n+1)]}}\right\} \\
e_{\mathrm{MF}}(m+1, n+1) &\equiv e_{\mathrm{MF}}\left[{}^{n}\mathfrak{w}_{\mathrm{MF}}, {}^{m+1,n+1}\mathfrak{w}_{\mathrm{MF}} - {}^{n}\mathfrak{w}_{\mathrm{MF}}\right] \qquad (14)
\end{aligned}
$$

The time-integration scheme is therefore defined by the triplet [CFL, CFL^*; M_{it}, r_{OBJ}], where either M_{it} or r_{OBJ} is specified.

Quasi-Newton Solver

The local dual-time-stepping method contains in the limit $\mathrm{CFL} \to \infty$ the quasi-Newton iteration, obtained by letting $\Delta t \to \infty$ [Eqs. (4–7)]

$$
{}^{n+1}\underline{\mathcal{L}}_{i,j,k} \cong 0 \quad \forall\, i, j, k \Longleftrightarrow \mathfrak{Q}({}^{n+1}\mathfrak{w}) \cong 0 \qquad (15)
$$

$$
\frac{{}^{m+1,n+1}\mathfrak{w} - {}^{m,n+1}\mathfrak{w}}{\Delta\mathfrak{t}^*} + \mathfrak{Q}({}^{m+1,n+1}\mathfrak{w}) \cong 0 \qquad (16)
$$

which is linearized, by Taylor-expanding $\mathfrak{Q}({}^{m+1,n+1}\mathfrak{w})$, as

$$
\begin{aligned}
&\frac{{}^{m+1,n+1}\mathfrak{w} - {}^{m,n+1}\mathfrak{w}}{\Delta\mathfrak{t}^*} + \mathfrak{Q}({}^{m,n+1}\mathfrak{w}) + \frac{\partial \mathfrak{Q}^J}{\partial \mathfrak{w}}({}^{m,n+1}\mathfrak{w}) \\
&\quad \times [{}^{m+1,n+1}\mathfrak{w} - {}^{m,n+1}\mathfrak{w}] \cong 0
\end{aligned} \qquad (17)
$$

and solved for ${}^{m+1,n+1}\mathfrak{w} - {}^{m,n+1}\mathfrak{w}$

$$
\begin{aligned}
&\left[\mathfrak{I} + \Delta\mathfrak{t}^{**}\frac{\partial \mathfrak{Q}^J}{\partial \mathfrak{w}}({}^{m,n+1}\mathfrak{w})\right][{}^{m+1,n+1}\mathfrak{w} - {}^{m,n+1}\mathfrak{w}] \\
&\quad \cong -\Delta\mathfrak{t}^{**}[\mathfrak{Q}({}^{m,n+1}\mathfrak{w})], \qquad \Delta\mathfrak{t}^{**} = \Delta\mathfrak{t}^*
\end{aligned} \qquad (18)
$$

The prefix "quasi" is added because approximate Jacobians are used in the iterative procedure. In the same way as the local dual-time-stepping approach [Eqs. (4–7)], the quasi-Newton time integration is characterized by the triplet [$\mathrm{CFL} = \infty$, CFL^*; M_{it}, r_{OBJ}], where either M_{it} or r_{OBJ} is specified. Note also that the simple alternating directions implicit approximate factorization (ADI-AF) integration without subiterations[10,61,62,67] is recovered by setting [CFL, CFL^*; M_{it}, r_{OBJ}] = [∞, CFL^*; 1, −]. This approach will not be used here because, although it will converge quite satisfactorily in many practical applications,[10,54] Chassaing et al.[13] have shown that subiterations are necessary to avoid limit-cycle oscillations when computing flows with large separation.

Multigrid Algorithm

Mean-Flow Multigrid and Operators

The multigrid algorithm is applied to the mean-flow variables $\mathfrak{w}_{\mathrm{MF}}$ only. Turbulence variables $\mathfrak{w}_{\mathrm{RSM}}$ are simply injected into coarser grids and are only updated on the fine grid (no multigrid increments for the turbulence variables).

To this purpose, it is useful to define a mean-flow subiteration operator ${}^{m}\boldsymbol{S}_{\mathrm{MF}}([{}^{m,n+1}\mathrm{w}_{\mathrm{MF}}, {}^{n}\mathrm{w}_{\mathrm{RSM}}], {}^{n}\mathrm{w}, \Delta\mathrm{t}, \Delta\mathrm{t}^{*}, \mathfrak{F}_{\mathrm{MF}})$, analogous to the subiteration operator ${}^{m}\boldsymbol{S}({}^{m,n+1}\mathrm{w}, {}^{n}\mathrm{w}, \Delta\mathrm{t}, \Delta\mathrm{t}^{*}, \mathfrak{F})$ [Eq. (9)]:

$$
\begin{aligned}
{}^{m+1,n+1}\mathrm{w}_{\mathrm{MF}} &= \boldsymbol{B}_{\mathrm{MF}}\Bigg\{ {}^{m,n+1}\mathrm{w}_{\mathrm{MF}} \\
&\quad - \left[\mathfrak{I} + \Delta\mathrm{t}^{**}\frac{\partial \mathfrak{Q}^{J}_{\mathrm{MF}}}{\partial \mathrm{w}_{\mathrm{MF}}}\left(\left[{}^{m,n+1}\mathrm{w}_{\mathrm{MF}}, {}^{n}\mathrm{w}_{\mathrm{RSM}}\right]\right)\right]^{-1}_{\mathrm{APPRX}} \\
&\quad \times \Delta\mathrm{t}^{**}\left[\mathfrak{R}_{\mathrm{MF}}\left(\left[{}^{m,n+1}\mathrm{w}_{\mathrm{MF}}, {}^{n}\mathrm{w}_{\mathrm{RSM}}\right], {}^{n}\mathrm{w}\right) + \mathfrak{F}_{\mathrm{MF}}\right]\Bigg\} \\
&\equiv {}^{m}\boldsymbol{S}_{\mathrm{MF}}\left(\left[{}^{m,n+1}\mathrm{w}_{\mathrm{MF}}, {}^{n}\mathrm{w}_{\mathrm{RSM}}\right], {}^{n}\mathrm{w}_{\mathrm{MF}}, \Delta\mathrm{t}, \Delta\mathrm{t}^{*}, \mathfrak{F}_{\mathrm{MF}}\right) \qquad (19)
\end{aligned}
$$

where $\mathfrak{Q}_{\mathrm{MF}}$ and $\mathfrak{Q}^{J}_{\mathrm{MF}}$ are the mean-flow equations space operator and the approximate space operator used for the Jacobians, and

$$
\begin{aligned}
&\mathfrak{R}_{\mathrm{MF}}\left(\left[{}^{m,n+1}\mathrm{w}_{\mathrm{MF}}, {}^{n}\mathrm{w}_{\mathrm{RSM}}\right], {}^{n}\mathrm{w}, \Delta\mathrm{t}\right) \\
&\quad = \left[\frac{{}^{m,n+1}\mathrm{w}_{\mathrm{MF}} - {}^{n}\mathrm{w}_{\mathrm{MF}}}{\Delta\mathrm{t}} + \mathfrak{Q}_{\mathrm{MF}}\left(\left[{}^{m,n+1}\mathrm{w}_{\mathrm{MF}}, {}^{n}\mathrm{w}_{\mathrm{RSM}}\right]\right)\right] \qquad (20)
\end{aligned}
$$

Full-iteration mean-flow operators $\boldsymbol{N}_{\mathrm{MF}}([\mathrm{w}_{\mathrm{MF}}, \mathrm{w}_{\mathrm{RSM}}], \mathrm{CFL}, \mathrm{CFL}^{*}, \mathfrak{F}_{\mathrm{MF}}; r_{\mathrm{OBJ}})$ and $\boldsymbol{N}_{\mathrm{MF}}([\mathrm{w}_{\mathrm{MF}}, \mathrm{w}_{\mathrm{RSM}}], \mathrm{CFL}, \mathrm{CFL}^{*}, \mathfrak{F}_{\mathrm{MF}}; M_{\mathrm{it}})$ are then defined in the same way as $\boldsymbol{N}$ [Eqs. (10) and (11)]:

$$
\begin{aligned}
&\{\textbf{do } m_{\mathrm{it}} = 1, M_{\mathrm{it}}, 1; m \equiv m_{\mathrm{it}}; {}^{m+1,n+1}\mathrm{w}_{\mathrm{MF}} \\
&\quad = {}^{m}\boldsymbol{S}_{\mathrm{MF}}\left(\left[{}^{m,n+1}\mathrm{w}_{\mathrm{MF}}, {}^{n}\mathrm{w}_{\mathrm{RSM}}\right], {}^{n}\mathrm{w}_{\mathrm{MF}}, \Delta\mathrm{t}, \Delta\mathrm{t}^{*}, \mathfrak{F}\right), \textbf{ end do}\} \\
&\quad \Longleftrightarrow {}^{n+1}\mathrm{w}_{\mathrm{MF}} \equiv {}^{M_{\mathrm{it}}+1,n+1}\mathrm{w}_{\mathrm{MF}} \\
&\quad = \boldsymbol{N}_{\mathrm{MF}}\left({}^{n}\mathrm{w}, \mathrm{CFL}, \mathrm{CFL}^{*}, \mathfrak{F}; M_{\mathrm{it}}\right) \qquad (21)
\end{aligned}
$$

$$
\begin{aligned}
&\{\textbf{do } m_{\mathrm{it}} \textbf{ while } [r_{\mathrm{MF}} \geq r_{\mathrm{OBJ}}]; m \equiv m_{\mathrm{it}}; {}^{m+1,n+1}\mathrm{w}_{\mathrm{MF}} \\
&\quad = \boldsymbol{S}_{\mathrm{MF}}\left(\left[{}^{m,n+1}\mathrm{w}_{\mathrm{MF}}, \mathrm{w}_{\mathrm{RSM}}\right], {}^{n}\mathrm{w}_{\mathrm{MF}}, \Delta\mathrm{t}, \Delta\mathrm{t}^{*}, \mathfrak{F}\right); \textbf{ end do}\} \\
&\quad \Longleftrightarrow {}^{n+1}\mathrm{w}_{\mathrm{MF}} \equiv {}^{r_{\mathrm{OBJ}},n+1}\mathrm{w}_{\mathrm{MF}} \\
&\quad = \boldsymbol{N}_{\mathrm{MF}}\left({}^{n}\mathrm{w}, \mathrm{CFL}, \mathrm{CFL}^{*}, \mathfrak{F}; r_{\mathrm{OBJ}}\right) \qquad (22)
\end{aligned}
$$

Restriction and Prolongation for Characteristic Multigrid

Leclercq and Stoufflet[71] have shown that, for a procedure with two levels of multigrid (fine + 1 coarse grid) with an upwind basic monogrid scheme, the upwind character of the scheme must be preserved in the multigrid procedure. This is obtained by respecting in the restriction (transfer from fine to coarse grid) operator for the residuals $\boldsymbol{T}^{2h}_{\mathfrak{R};h}$ the direction of propagation along characteristics (hence the term characteristic multigrid[71]), while using a geometric prolongation (interpolation from coarse to fine grid) operator for the increments $\boldsymbol{I}^{h}_{2h}$. The restriction operator for the variables $\boldsymbol{T}^{2h}_{\mathfrak{R};h}$ is a simple injection operator.[71] Leclercq and Stoufflet[71] developed their method for two arbitrarily nested unstructured grids. This algorithm is transposed in the present work to a structured grid, with the usual approach of obtaining coarser grids by omitting every other point, in each direction, of the finer grid.[30,39] These progressively coarser grids will be denoted $\mathcal{G}_h, \mathcal{G}_{2h}, \mathcal{G}_{4h}, \ldots$ ($\ell_{\mathrm{GRD}} = 1, 2, 3, \ldots$).

The restriction (transfer from fine to coarse grid) operator, for the flow-variables $\boldsymbol{T}^{2h}_{\mathfrak{R};h}$, is a simple injection operator

$$
\begin{aligned}
&\mathrm{w}_{2h} = \boldsymbol{T}^{2h}_{\mathrm{w};h}[\mathrm{w}_h] \\
&\Longleftrightarrow \underline{w}_{2h}(\underbrace{i_{2h}, j_{2h}, k_{2h}}_{n_{2h}}) = \underline{w}_{h}(\underbrace{i_h, j_h, k_h}_{n_h}) \\
&\quad \times \begin{cases} \forall \quad i_h = 1 + 2(i_{2h} - 1), & i_{2h} = 1, 2, \ldots, N_{i_{2h}} \\ \forall \quad j_h = 1 + 2(j_{2h} - 1), & j_{2h} = 1, 2, \ldots, N_{j_{2h}} \\ \forall \quad k_h = 1 + 2(k_{2h} - 1), & k_{2h} = 1, 2, \ldots, N_{k_{2h}} \end{cases} \qquad (23)
\end{aligned}
$$

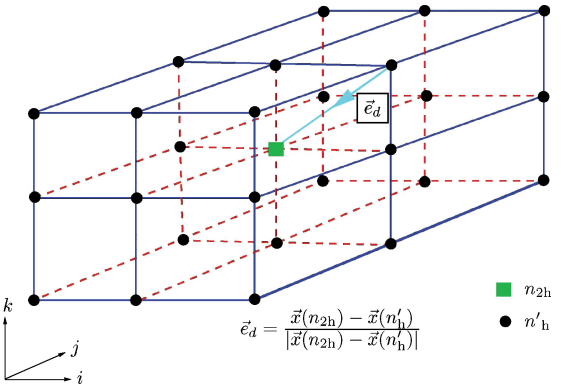

Fig. 1 Typical grid element illustrating the fine-grid neighbors n'_h of the coarse-grid point $n_{2h} \equiv n_h$ and the vector e_d, used in the construction of the matrix $\underline{\underline{\Phi}}$ [Eqs. (26–30)] of the characteristic multigrid restriction.[71]

The restriction (transfer from fine to coarse grid) operator, for the residuals and forcing terms, is the characteristic-transfer operator, introduced by Leclercq and Stoufflet.[71] The procedure is based on information propagation along characteristics. A coarse-grid point $n_{2h} = [i_{2h}, j_{2h}, k_{2h}] \in \mathcal{G}_{2h}$ receives information from the corresponding point $n_h = [i_h, j_h, k_h] \in \mathcal{G}_h$ [Eqs. (23)] and from the neighboring 26 points belonging to the eight $\mathcal{G}_h$ bricks having n_h as vertex (Fig. 1). These points will be denoted $n'_h \in \mathcal{M}_h(n_{2h})$, with $\mathcal{M}_h(n_{2h})$ the set

$$
\begin{aligned}
\mathcal{M}_h(n_{2h}) &= \mathcal{M}_{h_1}(n_{2h}) \cup \mathcal{M}_{h_2}(n_{2h}) \cup \mathcal{M}_{h_3}(n_{2h}) \\
&= \{[i_h \pm 1, j_h, k_h], [i_h, j_h \pm 1, k_h], [i_h, j_h, k_h \pm 1]\} \\
&\quad \cup \{[i_h \pm 1, j_h \pm 1, k_h], [i_h, j_h \pm 1, k_h \pm 1], \\
&\quad [i_h \pm 1, j_h, k_h \pm 1]\} \cup \{[i_h \pm 1, j_h \pm 1, k_h \pm 1]\} \qquad (24)
\end{aligned}
$$

For the present structured grid implementation, this operator can be written as

$$
\begin{aligned}
&\mathfrak{r}_{2h} = \boldsymbol{T}^{2h}_{\mathfrak{R};h}[\mathfrak{r}_h] \\
&\Longleftrightarrow \underline{r}_{2h}(n_{2h}) = \frac{1}{8}\underline{r}_h(n_h) + \sum_{n'_h \in \mathcal{M}_h(n_{2h})} \{\alpha(n'_h)\underline{\underline{\Phi}}(n_{2h}, n'_h)\underline{r}_h(n'_h)\} \\
&\quad \times \begin{cases} \alpha(n'_h) = \dfrac{1}{16}, & n'_h \in \mathcal{M}_{h_1}(n_{2h}) \\ \alpha(n'_h) = \dfrac{1}{32}, & n'_h \in \mathcal{M}_{h_2}(n_{2h}) \\ \alpha(n'_h) = \dfrac{1}{64}, & n'_h \in \mathcal{M}_{h_3}(n_{2h}) \end{cases} \qquad (25)
\end{aligned}
$$

The purpose of matrix $\underline{\underline{\Phi}} \in \mathbb{R}^{5\times 5}$ is to inhibit propagation of information in the wrong direction, along characteristics.[71] If $\underline{\underline{\Phi}} = \underline{\underline{I}}_5$, then the preceding restriction operator corresponds to simple centered collection of residuals (volume averaging on a uniform grid).[30,39,49] Instead, the matrix $\underline{\underline{\Phi}} = [\underline{\underline{P}}\ \underline{\underline{\Psi}}\ \underline{\underline{P}}^{-1}]$ is used. The matrices $\underline{\underline{P}}$, $\underline{\underline{P}}^{-1}$ are defined so as to diagonalize the Jacobian matrix of the inviscid fluxes along the direction $\boldsymbol{e}_d$ of the distance $\boldsymbol{x}(n_{2h}) - \boldsymbol{x}(n'_h)$. These matrices exist because of the hyperbolicity of the unsteady Euler equations and can be easily computed following Warming et al.,[72] who studied the diagonalization of flux Jacobians, both for conservative and nonconservative variables:

$$
\underline{\underline{A}}_d(n'_h) = \frac{\partial \underline{F}^{C}_{d}}{\partial \underline{w}} = \left[\underline{\underline{P}}\,\underline{\underline{\Lambda}}\,\underline{\underline{P}}^{-1}\right] \qquad (26)
$$

$$
\underline{F}^{C}_{d} = [\bar{\rho}\tilde{u}_d, \bar{\rho}\tilde{u}\tilde{u}_d + \bar{p}d_x, \bar{\rho}\tilde{v}\tilde{u}_d + \bar{p}d_y, \bar{\rho}\tilde{w}\tilde{u}_d + \bar{p}d_z, \bar{\rho}\tilde{u}_d\breve{h}_t]^{T}
$$

$$
\boldsymbol{e}_d = \frac{\boldsymbol{x}(n_{2h}) - \boldsymbol{x}(n'_h)}{|\boldsymbol{x}(n_{2h}) - \boldsymbol{x}(n'_h)|} \qquad (27)
$$

$$\underline{\underline{\Lambda}} = \mathrm{diag}\{\tilde{u}_d + \breve{a}, \tilde{u}_d, \tilde{u}_d, \tilde{u}_d, \tilde{u}_d - \breve{a}\}$$

$$\equiv \mathrm{diag}\{\lambda_1, \lambda_2, \lambda_3, \lambda_4, \lambda_5\} \tag{28}$$

where $u_d = \boldsymbol{V} \cdot \boldsymbol{e}_d$ is the velocity component along $\boldsymbol{e}_d$ (Fig. 1). The product $\underline{\underline{P}}^{-1}\underline{r}$ decomposes the residual to wave amplitudes along the characteristic directions.[66] If, for a given line of the diagonal matrix of eigenvalues $\underline{\underline{\Lambda}} = \mathrm{diag}\{\lambda_i;\, i = 1, \ldots, 5\}$, $\lambda_i \geq 0$, information corresponding to $[\underline{\underline{P}}^{-1}\underline{r}]_i$ propagates from point n'_h toward point n_{2h} and should be retained. On the other hand, if $\lambda_i < 0$, information does not propagate from point n'_h toward point n_{2h} and should be discarded. This is easily achieved by defining the matrix

$$\underline{\underline{\Psi}} = \tfrac{1}{2}\{\underline{\underline{I}}_5 + \mathrm{diag}[\mathrm{sgn}(\tilde{u}_d + \breve{a}), \mathrm{sgn}(\tilde{u}_d),$$

$$\mathrm{sgn}(\tilde{u}_d), \mathrm{sgn}(\tilde{u}_d), \mathrm{sgn}(\tilde{u}_d - \breve{a})]\} \tag{29}$$

whose diagonal entries are either 1 ($\lambda_i > 0$) or 0 ($\lambda_i < 0$). The choice

$$\underline{\underline{\Phi}} = [\underline{\underline{P}}\ \underline{\underline{\Psi}}\ \underline{\underline{P}}^{-1}] \tag{30}$$

has the desired property, when premultiplying $\underline{r}$, to initially transform to wave strengths ($\underline{\underline{P}}^{-1}\underline{r}$), then cut off information that would be propagated in the wrong direction ($\underline{\underline{\Psi}}\ \underline{\underline{P}}^{-1}\underline{r}$) and finally transform back to conservative residuals transmitted from point n'_h toward point n_{2h} ($\underline{\underline{\Phi}}\ \underline{r}$). In the original paper by Leclercq and Stoufflet,[71] the matrix $\underline{\underline{\Phi}}$ was further modified to ensure conservation (this requires a dynamic rescalling of $\underline{\underline{\Psi}}$. Numerical experiments, both with the original formulation[71] and with the present expression [Eqs. (30)], which does not preserve conservation, indicated that ensuring conservation for the restriction operator was not necessary. Furthermore, using the original conservative formulation induced premature saturation of residuals and delayed convergence. All of the results presented in this paper use the preceding form of $\underline{\underline{\Phi}}$ [Eq. (30)].

Finally, the prolongation (interpolation from coarse to fine grid) operator, for the increments $\Delta\mathfrak{w}$, $\boldsymbol{I}^h_{2h}$ is a standard geometric trilinear interpolation operator, used by many authors.[30,39,49]

Multigrid Algorithm

The multigrid algorithm is a standard FAS method, based on a fixed sawtooth cycle, with appropriate forcing terms.[31,39] Noting $\mathcal{G}_h$, $\mathcal{G}_{2h}$, $\mathcal{G}_{4h}$, the fine and successively coarser grids, the multigrid algorithm can be written, for three levels of multigrid ($L_{\mathrm{GRD}} = 3$), as follows.

Compute on $\mathcal{G}_h$:

$$\mathfrak{u}_h = {}^n\mathfrak{w}, \qquad \mathfrak{F}_h = 0, \qquad \mathfrak{v}_h = \boldsymbol{N}_h(\mathfrak{u}_h, \mathrm{CFL}, \mathrm{CFL}^*, \mathfrak{F}_h, r_{\mathrm{OBJ}}) \tag{31}$$

Transfer to $\mathcal{G}_{2h}$:

$$\begin{cases} \mathfrak{u}_{2h} = \boldsymbol{T}^{2h}_{\mathfrak{w};h}[\mathfrak{v}_h] \\ \mathfrak{F}_{\mathrm{MF}_{2h}} = \boldsymbol{T}^{2h}_{\mathfrak{R};h}[\mathfrak{Q}_{\mathrm{MF}_h}(\mathfrak{v}_h)] - \mathfrak{Q}_{\mathrm{MF}_{2h}}(\mathfrak{u}_{2h}) \end{cases} \tag{32}$$

Compute on $\mathcal{G}_{2h}$:

$$\begin{cases} \mathfrak{v}_{\mathrm{MF}_{2h}} = \boldsymbol{N}_{\mathrm{MF}_{2h}}(\mathfrak{u}_{2h}, \mathrm{CFL}, \mathrm{CFL}^*, \mathfrak{F}_{2h}, r_{\mathrm{OBJ}}) \\ \mathfrak{v}_{\mathrm{RSM}_{2h}} = \mathfrak{u}_{\mathrm{RSM}_{2h}} = \boldsymbol{T}^{2h}_{\mathfrak{w};h}[\mathfrak{v}_{\mathrm{RSM}_h}] \end{cases} \tag{33}$$

Transfer to $\mathcal{G}_{4h}$:

$$\begin{cases} \mathfrak{u}_{4h} = \boldsymbol{T}^{4h}_{\mathfrak{w};2h}[\mathfrak{v}_{2h}] \\ \mathfrak{F}_{\mathrm{MF}_{4h}} = \boldsymbol{T}^{4h}_{\mathfrak{R};2h}[\mathfrak{Q}_{\mathrm{MF}_{2h}}(\mathfrak{v}_{2h}) + \mathfrak{F}_{\mathrm{MF}_{2h}}] - \mathfrak{Q}_{\mathrm{MF}_{4h}}(\mathfrak{u}_{4h}) \end{cases} \tag{34}$$

Compute on $\mathcal{G}_{4h}$:

$$\begin{cases} \mathfrak{v}_{\mathrm{MF}_{4h}} = \boldsymbol{N}_{\mathrm{MF}_{4h}}(\mathfrak{u}_{4h}, \mathrm{CFL}, \mathrm{CFL}^*, \mathfrak{F}_{\mathrm{MF}_{4h}}, r_{\mathrm{OBJ}}) \\ \mathfrak{v}_{\mathrm{RSM}_{4h}} = \mathfrak{u}_{\mathrm{RSM}_{4h}} = \boldsymbol{T}^{4h}_{\mathfrak{w};2h}[\mathfrak{v}_{\mathrm{RSM}_{2h}}] \end{cases} \tag{35}$$

Interpolation:

$${}^{n+1}\mathfrak{w} = \boldsymbol{B}_h\left\{\mathfrak{v}_h + \boldsymbol{I}^h_{2h}[\mathfrak{v}_{2h} - \mathfrak{u}_{2h}] + \boldsymbol{I}^h_{2h}\boldsymbol{I}^{2h}_{4h}[\mathfrak{v}_{4h} - \mathfrak{u}_{4h}]\right\} \tag{36}$$

In these relations $\mathfrak{u}$, $\mathfrak{v}$, and $\mathfrak{F}$ are internal variables and were not superscripted. The variables $\mathfrak{u}_h$, $\mathfrak{u}_{2h}$, and $\mathfrak{u}_{4h}$ are initial values, at the beginning of the computation on the corresponding grid. (They are obtained by restriction from the immediately finer grid.) The variables $\mathfrak{v}_h$, $\mathfrak{v}_{2h}$, and $\mathfrak{v}_{4h}$ are final values, obtained on the corresponding grid from the application of the full iteration $\boldsymbol{N}$. The quantities $\mathfrak{F}_h \equiv 0$, $\mathfrak{F}_{\mathrm{MF}_{2h}}$, and $\mathfrak{F}_{\mathrm{MF}_{4h}}$ are the forcing terms on the corresponding grids, ensuring that the procedure is driven by the fine-grid residuals, so that the multigrid results are exactly the same as those of a monogrid computation. For a higher number of grids, the $\mathcal{G}_{4h}$ step would be repeated on $\mathcal{G}_{8h}$.

The algorithm has been successfully applied for flows up to $M = 3$, with three levels of multigrid (fine + 2 coarser grids). Running with four levels of multigrid was successful for $M < 2$ but not for $M = 3$. At high Mach numbers, some damping of the residuals in the restriction operator is necessary, as has been shown by Gerlinger and coworkers[23,25] and Radespiel and Swanson.[73]

Application to Two-Equation Closures

The just presented monogrid and multigrid algorithms are readily applicable to any transport-equations turbulence model. For all mean-flow gradient-based models, such as one- or two-equation closures, whether they use a linear Boussinesq relation or nonlinear closures,[29,74] the turbulence variables that are injected into the coarser grids are not the Reynolds stresses, but the turbulence velocity and timescales, such as k–ε or k–ω_T or ν_T.

The Reynolds stresses, on the coarser grid, are recomputed in the space operator $\mathfrak{Q}_{\mathrm{MF}_{2h}}$ using the mean-flow gradients evaluated on the coarse grid. For a k–ε linear Boussinesq closure, this operation reads

$$[\bar{\rho}\widetilde{u''_i u''_j}]_{2h} = \frac{2}{3}\rho k_h \delta_{ij} - [\mu_T]_h\left[\frac{\partial \tilde{u}_i}{\partial x_j} + \frac{\partial \tilde{u}_j}{\partial x_i} - \frac{2}{3}\frac{\partial \tilde{u}_\ell}{\partial x_\ell}\right]_{2h}$$

$$[\bar{\rho}\widetilde{u''_i u''_j}]_{4h} = \frac{2}{3}\rho k_h \delta_{ij} - [\mu_T]_h\left[\frac{\partial \tilde{u}_i}{\partial x_j} + \frac{\partial \tilde{u}_j}{\partial x_i} - \frac{2}{3}\frac{\partial \tilde{u}_\ell}{\partial x_\ell}\right]_{4h} \tag{37}$$

$$[\bar{\rho}\widetilde{h'' u''_i}]_{2h} = [\kappa_T]_h\left[\frac{\partial \tilde{T}}{\partial x_i}\right]_{2h}, \qquad \left[\bar{\rho}\widetilde{h'' u''_i}\right]_{4h} = [\kappa_T]_h\left[\frac{\partial \tilde{T}}{\partial x_i}\right]_{4h} \tag{38}$$

When using a k–ε model, it is necessary to use the preceding relations to obtain with the multigrid algorithm the same results as with the monogrid algorithm. Incidentally, the relation for the heat fluxes [Eqs. (38)] is also used in the Reynolds-stress closure. On the contrary, when using a seven-equation RSM closure, Reynolds stresses are simply injected from the fine grid:

$$[\bar{\rho}\widetilde{u''_i u''_j}]_{2h} = [\bar{\rho}\widetilde{u''_i u''_j}]_h, \qquad [\bar{\rho}\widetilde{u''_i u''_j}]_{4h} = [\bar{\rho}\widetilde{u''_i u''_j}]_h \tag{39}$$

Results

Configurations Studied

To assess the independence of multigrid convergence acceleration on the particular turbulence model used, results are systematically presented using three different near-wall low-turbulence Reynolds-number closures: 1) the widely used Launder–Sharma[28] two-equation k–ε (denoted LS k–ε), which is known to underestimate separation,[10,18,52,75] 2) the wall-topology-independent (wall-normal-free) Gerolymos–Vallet[51] seven-equation RSM (denoted GV RSM), which slightly overpredicts separation,[52,75] and 3) the wall-normal-free version[52] of the Launder–Shima–Sharma[10] seven-equation RSM (denoted WNF–LSS RSM), developed in Gerolymos et al.,[52] which slightly underpredicts separation.

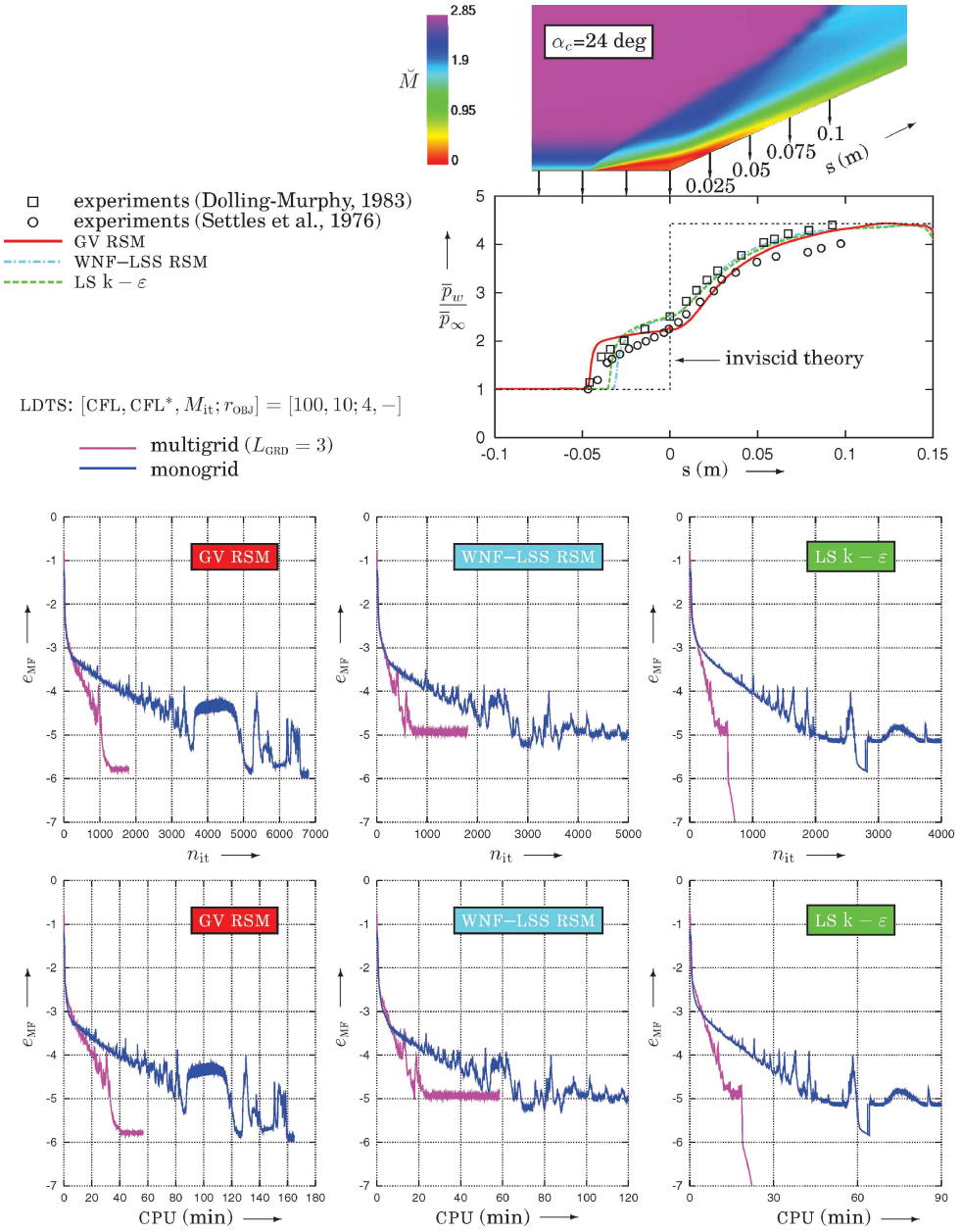

Fig. 2 Convergence of mean-flow error e_{MF}, as a function of the number of iterations n_{it} and of CPU time (for a 2-Gflop sustained performance), using monogrid (L_{GRD} = 1) and multigrid (L_{GRD} = 3) algorithms, for the α_c = 24 deg compression-ramp interaction of Settles et al.[55] and Dolling and Murphy[56] [M_∞ = 2.85, Re_{δ_0} = 1.33 × 10^6; iso-Machs computed with the GV (Ref. 51) RSM; comparison of wall-pressure distributions with experimental measurements; 401 × 201 grid_A (Ref. 75) using the GV (Ref. 51) and WNF–LSS (Ref. 52) wall-normal-free RSMs, and the Launder–Sharma[28] k–ε model, with an LDTS integration strategy ([CFL, CFL*; M_{it}, r_{OBJ}] = [100, 10; 4, −]).

The proposed multigrid strategy was evaluated by computing two different configurations: 1) a compression-ramp configuration ($M_{SW} = 2.85, \alpha_c = \Delta\vartheta_{SW} = 24$ deg, $Re_{\theta_0} = 8 \times 10^4$) studied experimentally by Settles el al.[55] and Dolling and Murphy[56] for which two-dimensional computations are presented, and 2) a high-subsonic (inflow Mach number $M_i \sim 0.6$) annular cascade, with large separation, studied experimentally by Doukelis et al.,[58,59] for which three-dimensional multidomain computations are presented.

M = 2.85 Compression Ramp

A first evaluation of the multigrid method is performed for a $M_\infty = 2.85$ oblique-shock-wave/turbulent-boundary-layer interaction, on a $\alpha_c = 24$ deg compression ramp, studied experimentally by Settles et al.[55] and Dolling and Murphy[56] An extended separation is observed (Fig. 2), inducing a substantial upstream influence of the interaction, which is clearly visible in the wall-pressure distribution (Fig. 2). The authors[75] have computed this configuration using a monogrid algorithm[13] and have presented systematic comparisons with available experimental measurements.[75] This previous work[75] includes a careful grid-convergence study, which indicates that a 401 × 201 (grid_A in Gerolymos–Sauret–Vallet[75]) computational grid gives satisfactory results (although not completely grid converged).

Computations using the two wall-normal-free RSMs [GV (Ref. 51) RSM and WNF–LSS (Ref. 52) RSM] and the LS (Ref. 28) k–ε model were run with a LDTS ([CFL, CFL*; M_{it}, r_{OBJ}] = [100, 10; 4, −]) integration strategy, both in monogrid mode and with three levels of multigrid ($L_{GRD} = 3$; fine + 2 coarser grids). The monogrid convergence (Fig. 2) is slower for the GV (Ref. 51) RSM, which predicts, in accordance with measurements, large separation, and faster with the WNF–LSS (Ref. 52) RSM and the LS (Ref. 28) k–ε models, which underestimate separation. This

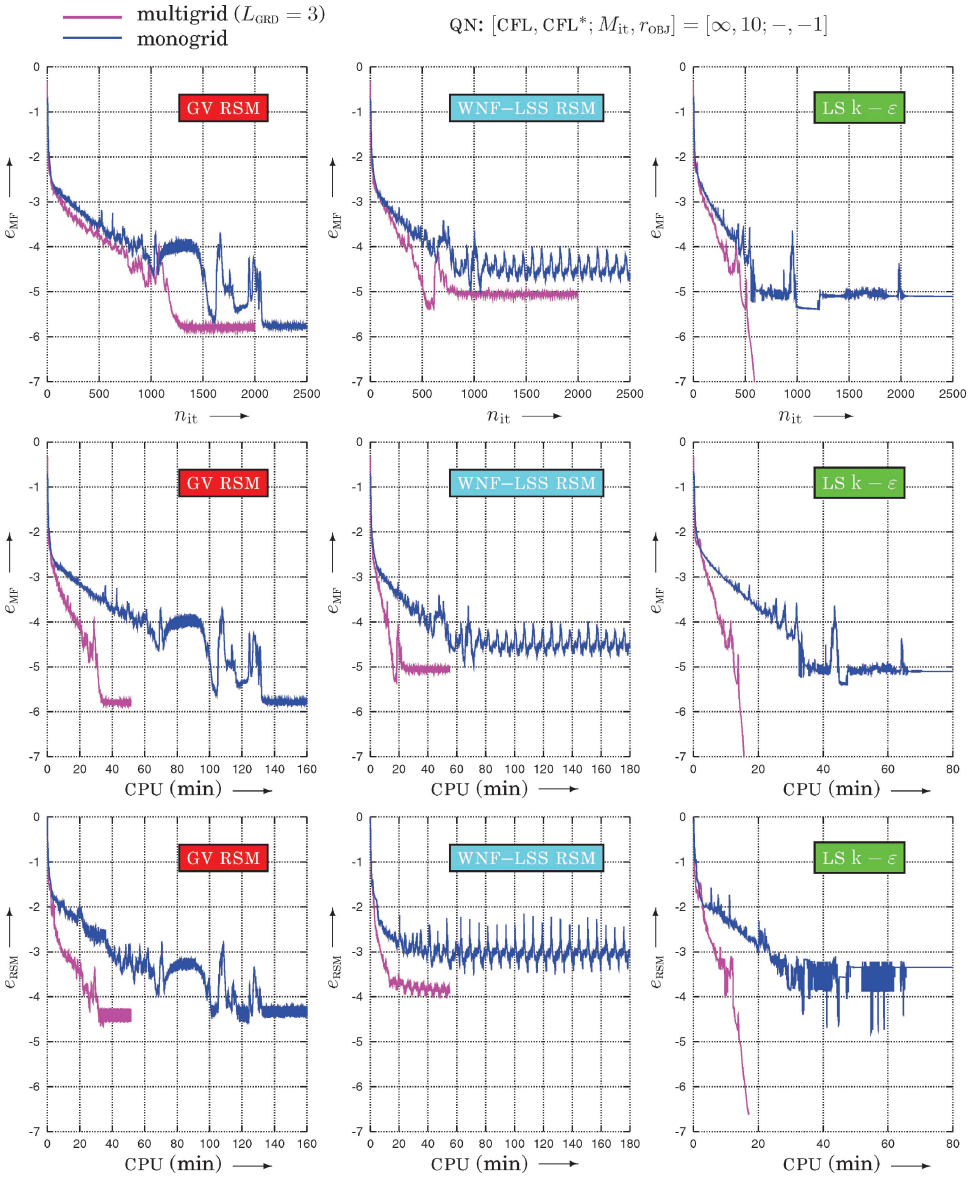

Fig. 3 Convergence of mean-flow error e_{MF} and of turbulence-variables error e_{RSM}, as a function of the number of iterations n_{it} and of CPU time (for a 2-Gflop sustained performance), using monogrid ($L_{GRD} = 1$) and multigrid ($L_{GRD} = 3$) algorithms, for the $\alpha_c = 24$ deg compression-ramp interaction of Settles et al.[55] and Dolling and Murphy[56] [$M_\infty = 2.85$, $Re_{\delta_0} = 1.33 \times 10^6$; 401 × 201 grid_A (Ref. 75) using the GV (Ref. 51) and WNF–LSS (Ref. 52) wall-normal-free RSMs, and the Launder–Sharma[28] k–ε model, with a quasi-Newton integration strategy ([CFL, CFL*; M_{it}, r_{OBJ}] = [∞, 10; −, −1]).

is because of the higher complexity of the separated flow structure and the stronger shock-wave/boundary-layer interaction, which is predicted (in accordance with measurements) by the GV (Ref. 51) RSM. Multigrid computations (Fig. 2) are substantially faster for all of the three turbulence closures used, with speed-ups of ∼4 (3.8–4.5 depending on the turbulence model used). Multigrid and monogrid results are of course identical. Although the time to convergence is turbulence model dependent (the better the agreement of the model with the experimentally determined complex flow structure the largest the time to convergence), the relative speed-up of the various multigrid strategies is reasonably turbulence model independent.

Computations were also run using a more aggressive quasi-Newton ([CFL, CFL*; M_{it}, r_{OBJ}] = [∞, 10; −, −2]) integration strategy (Fig. 3), where a two orders-of-magnitude convergence reduction was required for the increments ($r_{OBJ} = -2$). Naturally the quasi-Newton strategy exhibits faster convergence (Fig. 3) than the corresponding computations with the LDTS strategy (Fig. 2). Again, a speed-up of ∼4 is obtained using three levels of multigrid (Fig. 3). Examination of the convergence of the turbulence variables e_{RSM} indicates (Fig. 3) a behavior very similar to the mean-flow variables e_{RSM}.

Multidomain Implementation and Subsonic Annular Cascade Flow

For realistic practical applications it is necessary to use multiblock grids.[76] In the approach followed by the authors, information is exchanged between blocks (Fig. 4) using a phantom-nodes technique.[57] For monogrid applications $N_{PH} = 5$ phantom nodes were used, so as to be able to apply simple no-change implicit boundary conditions[65] at the phantom boundary, without contaminating the solution. A typical example is the computation of three-dimensional flow through an annular subsonic stator (nonrotating) cascade, which was studied experimentally by Doukelis et al.,[59] and served as a test case for the development of the basic monogrid scheme with RSM closure.[13] The flow is characterized by a large hub corner stall, creating a large recirculating flow region. The associated blockage induces negative flow turning near the hub (Fig. 5). Previous studies[54] have highlighted the superiority of RSM closures in predicting this flow, compared to two-equation models (Fig. 5).

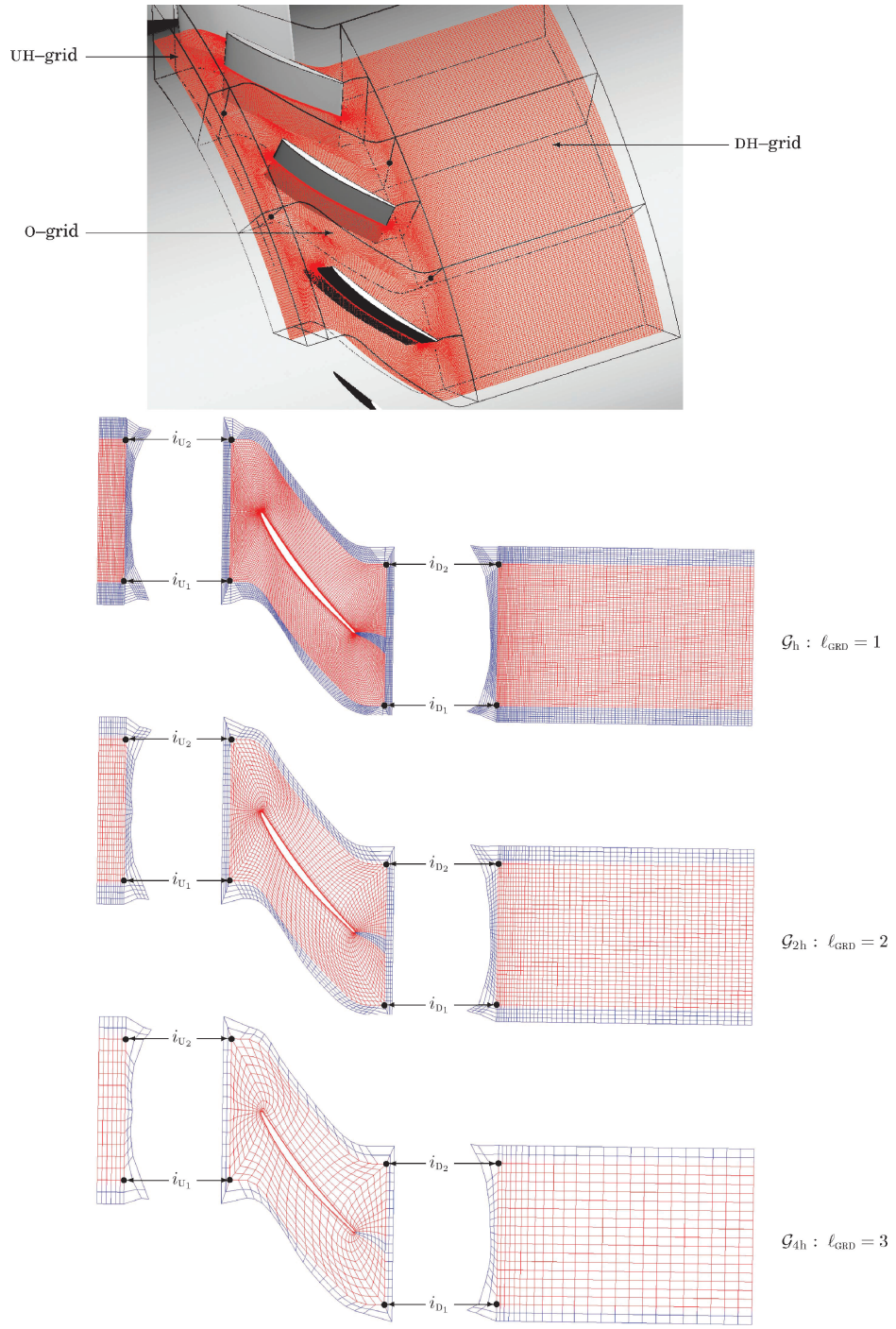

Fig. 4 View of three-dimensional computational grid, at midspan, for the National Technical University of Athens (NTUA) annular cascade,[59] and grid domains (in red) with phantom nodes (in blue), at midspan, for the fine ($\ell_{GRD} = 1$) and coarser grids ($\ell_{GRD} = 2,3$), illustrating that grid-domain corners ($i_{U_1}, i_{U_2}, i_{D_1}, i_{D_2}$) belong to the entire sequence of grids ($\mathcal{G}_h, \mathcal{G}_{2h}, \mathcal{G}_{4h}$).

The computational grid is an H–O–H three-block grid (Fig. 4), generated biharmonically.[77] To apply the multigrid strategy just described, the number of phantom nodes was increased to $N_{PH} = 8 = 2^3$, which allows multigrid coarsening for three levels of multigrid ($L_{GRD} = 3$). It is also necessary to built the fine grid so as to ensure block connectivity of the coarser grids. To this purpose, it is necessary that the corners of the computational grid boundaries[77] belong to the entire multigrid sequence of progressively coarser grids $\mathcal{G}_h$, $\mathcal{G}_{2h}$, and $\mathcal{G}_{4h}$. The grid-generation module adjusts the corresponding grid points[77] (Fig. 4) to

$$i_{U_1} - 1 \propto 2^{L_{GRD}-1}, \qquad i_{U_2} - 1 \propto 2^{L_{GRD}-1}$$
$$i_{D_1} - 1 \propto 2^{L_{GRD}-1}, \qquad i_{D_2} - 1 \propto 2^{L_{GRD}-1} \tag{40}$$

in the same way as the number of grid-points (N_i, N_j, N_k) for each grid-block. In this way the interfaces between grid-blocks are defined on the entire multigrid sequence of grids (Fig. 4).

For this configuration, computations using the three different turbulent closures were run on a 2.75×10^6 H–O–H grid (grid_DE in Chassaing et al.[13]), both in monogrid ($L_{GRD} = 1$) and multigrid mode ($L_{GRD} = 3$). Considering the convergence of mass flow at the cascade inlet $\dot{m}_i$ as a function of CPU time, using a LDTS ([CFL, CFL*, M_{it}; r_{OBJ}] = [100, 10; −, −1]) integration strategy, indicates that a speed-up of ∼3 is obtained for all three models (Fig. 5). Analogous results are obtained by using a quasi-Newton ([CFL, CFL*, M_{it}; r_{OBJ}] = [∞, 10; −, −2]) integration strategy (Fig. 6).

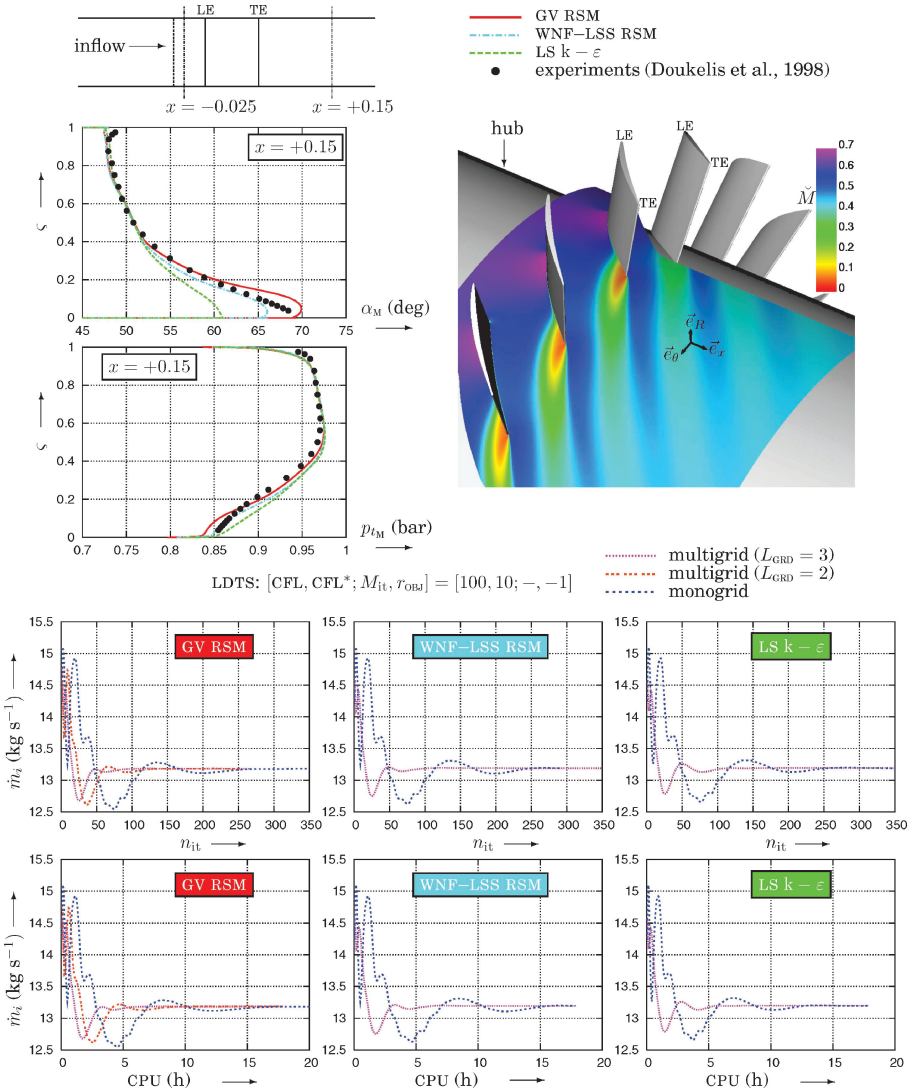

Fig. 5 Convergence of mass flow at cascade inlet $\dot{m}_i$ (kgs^{-1}) as function of the number of iterations n_{it} and CPU time (for a 2-Gflop sustained performance), using monogrid ($L_{GRD} = 1$) and multigrid ($L_{GRD} = 2,3$) algorithms, for the NTUA annular cascade[59] [$\dot{m} = 13.2$ kg s^{-1}; $T_{u_i} = 4\%$; $\ell_{T_i} = 0.04$ m; 2.75×10^6 grid_DE (Ref. 13); Mach contours computed with the GV (Ref. 51) RSM, and comparison of measured[59] and computed spanwise [ς] distributions of pitchwise-averaged flow angle α_{M_o} and pitchwise-averaged total pressure $p_{t_{M_o}}$ at the outlet of the cascade; the $xR\theta$ frame on the iso-Machs is located at the $x = +0.15$ m outlet station], using the GV (Ref. 51) and WNF–LSS (Ref. 52) wall-normal-free RSMs, and the Launder–Sharma[28] k–ε model, and an LDTS iteration strategy ([CFL, CFL*, M_{it}; r_{OBJ}] = [100, 10; −, −1]).

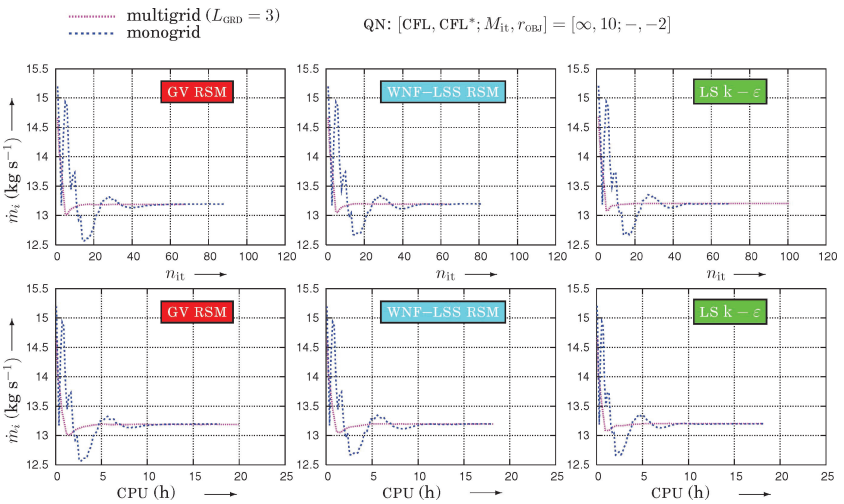

Fig. 6 Convergence of mass flow at cascade inlet $\dot{m}_i$ (kgs^{-1}) as function of the number of iterations n_{it} and CPU time (for a 2-Gflop sustained performance), using monogrid ($L_{GRD} = 1$) and multigrid ($L_{GRD} = 3$) algorithms, for the NTUA annular cascade[59] [$\dot{m} = 13.2$ kg s^{-1}; $T_{u_i} = 4\%$; $\ell_{T_i} = 0.04$ m; 2.75×10^6 grid_DE (Ref. 13)], using the GV (Ref. 51) and WNF–LSS (Ref. 52) wall-normal-free RSMs, and the Launder–Sharma[28] k–ε model, and a quasi-Newton iteration strategy ([CFL, CFL*, M_{it}; r_{OBJ}] = [∞, 10; −, −2]).

Conclusions

In the present paper the acceleration of three-dimensional compressible Navier–Stokes computations with advanced seven-equation Reynolds-stress model (RSM) turbulence closures, by applying multigrid to the mean-flow variables only, is examined with the following conclusions:

1) Based on an implicit upwind-biased $\mathcal{O}(\Delta x^3)$ basic monogrid scheme, a sawtooth-cycle FAS multigrid was applied to the mean-flow variables only, using characteristic multigrid for the restriction operator, to maintain the upwind character of the baseline scheme. The Reynolds stresses were computed on the finest grid only and were simply injected into progressively coarser grids. This technique minimizes the complexity of source terms treatment during the multigrid sequence.

2) The technique was also applied for two-equation k–ε models, by injecting k and ε into progressively coarser grids, and recomputing Reynolds stresses and heat fluxes using mean-flow gradients evaluated on the coarse grid. This is necessary, both for stability and for ensuring that multigrid and monogrid results are identical. Note that turbulence heat fluxes are evaluated in this way for the RSM computations also, where a gradient heat-flux-model was used.

3) Tests on various two- and three-dimensional configurations over a wide range on Mach numbers (0–3), including complex three-dimensional flows with large separation and multiblock grids, demonstrate that this simple multigrid augmentation achieves speed-ups of 3–4, using three levels of multigrid (fine + 2 coarser grids). This speed-up is obtained both with seven-equation RSM and with two-equation closures and is reasonably turbulence model independent.

4) Results computed using the present mean-flow multigrid technique were invariably identical to those obtained by monogrid calculations. The mean-flow multigrid technique is very robust and, in contradiction with some previous reports in the literature, has successfully accelerated the computations for all of the tests studied by the authors.

Further work should concentrate on efficient multigrid techniques to include the turbulence variables in the multigrid procedure, based on the guidelines stated in the Introduction.

Acknowledgments

The computations presented in this work were run at the Institut pour le Développement des Ressources en Informatique Scientifique. The authors are listed alphabetically. The numerical methodology described in the present paper was implemented in the RSM_3D software developed by the authors.

References

[1]Hanjalić, K., "Advanced Turbulence Closure Models: A View of Current Status and Future Prospects," *International Journal of Heat Fluid Flow*, Vol. 15, No. 3, 1994, pp. 178–203.

[2]Vandromme, D., and Minh, H. H., "About the Coupling of Turbulence Closure Models with Averaged Navier–Stokes Equations," *Journal of Computational Physics*, Vol. 65, No. 2, 1986, pp. 386–409.

[3]Morrison, J. H., "A Compressible Navier–Stokes Solver with 2-Equation and Reynolds-Stress Turbulence Closure Models," NASA CR-4440, 1992; also AIAA Paper 90-5251, Oct. 1990.

[4]Lien, F. S., and Leschziner, M. A., "A Pressure-Velocity Solution Strategy for Compressible Flow and its Application to Shock/Boundary-Layer Interaction Using Second-Moment Closure," *Journal of Fluids Engineering*, Vol. 115, Dec. 1993, pp. 717–725.

[5]Chuang, C. C., and Chieng, C. C., "Comparison of Varients of the Bi-Conjugate Gradient Method for Compressible Navier–Stokes with 2-Moment Closure," *International Journal for Numerical Methods in Fluids*, Vol. 20, 1995, pp. 233–253.

[6]Davidson, L., "Reynolds-Stress Transport Modelling of Shock-Induced Separated Flow," *Computers and Fluids*, Vol. 24, No. 3, 1995, pp. 253–268.

[7]Leschziner, M. A., "Computation of Aerodynamic Flows with Turbulence-Transport Models Based on 2-Moment Closure," *Computers and Fluids*, Vol. 24, No. 4, 1995, pp. 377–392.

[8]Ladeinde, F., "Supersonic Flux-Split Procedure for Second Moments of Turbulence," *AIAA Journal*, Vol. 33, No. 7, 1995, pp. 1185–1195.

[9]Zha, G. C., and Knight, D. D., "Three-Dimensional Shock/Boundary-Layer Interaction Using Reynolds Stress Equation Turbulence Model," *AIAA Journal*, Vol. 34, No. 7, 1996, pp. 1313–1320.

[10]Gerolymos, G. A., and Vallet, I., "Near-Wall Reynolds-Stress Three-Dimensional Transonic Flows Computation," *AIAA Journal*, Vol. 35, No. 2, 1997, pp. 228–236.

[11]Chenault, C. F., Beran, P. S., and Bowersox, R. D. W., "Numerical Investigation of Supersonic Injection Using a Reynolds-Stress Turbulence Model," *AIAA Journal*, Vol. 37, No. 10, 1999, pp. 1257–1269.

[12]Batten, P., Craft, T. J., Leschziner, M. A., and Loyau, H., "Reynolds-Stress-Transport Modeling for Compressible Aerodynamics Applications," *AIAA Journal*, Vol. 37, No. 7, 1999, pp. 785–797.

[13]Chassaing, J. C., Gerolymos, G. A., and Vallet, I., "Efficient and Robust Reynolds-Stress Model Computation of Three-Dimensional Compressible Flows," *AIAA Journal*, Vol. 41, No. 5, 2003, pp. 763–773.

[14]Hirsch, C., *Numerical Computation of Internal and External Flows*, 1st ed., Vol. 2, Wiley, New York, 1990, pp. 224–296, 493–594, 661–670.

[15]Brandt, A., "Multilevel Adaptive Solutions to Boundary-Value Problems," *Mathematics of Computations*, Vol. 31, No. 138, 1977, pp. 330–390.

[16]Demuren, A. O., "Multigrid Acceleration and Turbulence Models for Computations of 3-D Turbulence Jets in Crossflow," *International Journal of Heat and Mass Transfer*, Vol. 35, No. 11, 1992, pp. 2783–2794.

[17]Lien, F. S., and Leschziner, M. A., "Multigrid Acceleration for Recirculating Laminar and Turbulent Flows Computed with a Non-Orthogonal Collocated Finite-Volume Scheme," *Computer Methods in Applied Mechanics and Engineering*, Vol. 118, No. 3–4, 1994, pp. 351–371.

[18]Gerolymos, G. A., "Implicit Multiple-Grid Solution of the Compressible Navier–Stokes Equations Using k–ε Turbulence Closure," *AIAA Journal*, Vol. 28, No. 10, 1990, pp. 1707–1717.

[19]Sikonen, T., "An Application of Roe's Flux-Difference Splitting for k–ε Turbulence Model," *International Journal for Numerical Methods in Fluids*, Vol. 21, 1995, pp. 1017–1039.

[20]Liu, F., and Zheng, X., "A Strongly Coupled Time-Marching Method for Solving the Navier–Stokes and k–ω Turbulence Model Equations with Multigrid," *Journal of Computational Physics*, Vol. 128, No. 2, 1996, pp. 289–300; also AIAA Paper 94-2389, Oct. 1994.

[21]Dick, E., and Steelant, J., "Coupled Solution of the Steady Compressible Navier–Stokes and k–ε Turbulence Equations with a Multigrid Method," *Applied Numerical Mathematics*, Vol. 23, No. 1, 1997, pp. 49–61.

[22]Gerlinger, P., and Brüggemann, D., "Multigrid Convergence Acceleration for Turbulent Supersonic Flows," *International Journal for Numerical Methods in Fluids*, Vol. 24, No. 10, 1997, pp. 1019–1035.

[23]Gerlinger, P., and Brüggemann, D., "An Implicit Multigrid Scheme for the Compressible Navier–Stokes Equations with Low-Reynolds-Number Turbulence Closure," *Journal of Fluids Engineering*, Vol. 120, No. 2, 1998, pp. 257–262.

[24]Lin, H., and Chieng, C. C., "Computations of Transonic Turbulent Flow past Airfoils Using Multigrid/Bi-CGSTAB Algorithm," *AIAA Journal*, Vol. 37, No. 1, 1999, pp. 118–121.

[25]Gerlinger, P., Stoll, P., and Brüggemann, D., "Robust Implicit Multigrid Method for the Simulation of Turbulent Supersonic Mixing," *AIAA Journal*, Vol. 37, No. 6, 1999, pp. 766–768.

[26]Lambropoulos, N. K., Koubogiannis, D. G., and Giannakoglou, K. C., "Acceleration of a Navier–Stokes Equation Solver for Unstructured Grids Using Agglomeration Multigrid and Parallel Processing," *Computer Methods in Applied Mechanics and Engineering*, Vol. 193, No. 9, 2004, pp. 781–803.

[27]Kunz, R. F., and Lakshminarayana, B., "Stability of Explicit Navier–Stokes Procedures Using k–ε and k–ε/Algebraic-Reynolds-Stress Turbulence Models," *Journal of Computational Physics*, Vol. 103, No. 1, 1992, pp. 141–159.

[28]Patel, V. G., Rodi, W., and Scheuerer, G., "Turbulence Models for Near-Wall and Low-Reynolds-Number Flows: A Review," *AIAA Journal*, Vol. 23, No. 9, 1985, pp. 1308–1319.

[29]Wilcox, D. C., *Turbulence Modelling for CFD*, 2nd ed., DCW Industries, La Cañada, CA, 1998, pp. 119–123, 273–284.

[30]Ni, R. H., "A Multiple Grid Scheme for Solving the Euler Equations," *AIAA Journal*, Vol. 20, No. 11, 1982, pp. 1565–1571.

[31]Jameson, A., and Yoon, S., "Multigrid Solution of the Euler Equations Using Implicit Schemes," *AIAA Journal*, Vol. 24, No. 11, 1986, pp. 1737–1743.

[32]Liu, F., and Ji, S., "Unsteady Flow Calculations with a Multigrid Navier–Stokes Method," *AIAA Journal*, Vol. 34, No. 10, 1996, pp. 2047–2053.

[33]Rumsey, C. L., Sanetrik, M. D., Bierdon, R. T., Melson, N. D., and Parlette, E. B., "Efficiency and Accuracy of Time-Accurate Turbulent Navier–Stokes Computations," *Computers and Fluids*, Vol. 25, No. 2, 1996, pp. 217–236.

[34]Dubuc, L., Cantariti, F., Woodgate, M., Gribben, B., Badcock, K. J., and Richards, B. E., "Solution of the Unsteady Euler Equations Using an Implicit Dual-Time Method," *AIAA Journal*, Vol. 36, No. 8, 1998, pp. 1417–1424.

[35]Caughey, D. A., "Implicit Multigrid Computation of Unsteady Flows past Cylinders of Square Cross-Section," *Computers and Fluids*, Vol. 30, No. 7–8, 2001, pp. 939–960.

[36]Chassaing, J. C., Gerolymos, G. A., and Vallet, I., "Reynolds-Stress Model Dual-Time-Stepping Computation of Unsteady Three-Dimensional Flows," *AIAA Journal*, Vol. 41, No. 10, 2003, pp. 1882–1894.

[37]Liu, F., and Jameson, A., "Multigrid Navier–Stokes Calculations for 3-D Cascades," *AIAA Journal*, Vol. 31, No. 10, 1993, pp. 1785–1791.

[38]Liu, F., and Zheng, X., "Staggered Finite-Volume Scheme for Solving Cascade Flow with a k–ω Turbulence Model," *AIAA Journal*, Vol. 32, No. 8, 1994, pp. 1589–1597.

[39]Jameson, A., "Solution of the Euler Equations for 2-D Transonic Flow by a Multigrid Method," *Applied Mathematics and Computation*, Vol. 13, Nos. 3–4, 1983, pp. 327–355.

[40]Park, S. H., and Kwon, J. H., "Implementation of k–ω Turbulence Models in an Implicit Multigrid Method," *AIAA Journal*, Vol. 42, No. 7, 2004, pp. 1348–1357.

[41]Steelant, J., Dick, E., and Pattijn, S., "Multigrid Methods for Compressible Navier–Stokes Equations in Low-Speed Flows," *Journal of Computational and Applied Mathematics*, Vol. 82, No. 1–2, 1997, pp. 379–388.

[42]Coakley, T. J., "Turbulence Modeling Methods for Compressible Navier–Stokes Equations," AIAA Paper 83-1693, June 1983.

[43]Lallemand, M.-H., Steve, H., and Dervieux, A., "Unstructured Multigridding by Volume Agglomeration: Current Status," *Computers and Fluids*, Vol. 21, No. 3, 1992, pp. 397–433.

[44]Mavriplis, D. J., "An Assessment of Linear Versus Nonlinear Multigrid Methods for Unstructured Mesh Solvers," *Journal of Computational Physics*, Vol. 175, No. 1, 2002, pp. 302–325; also AIAA Paper 2001-2573, Jan. 2001.

[45]Carré, G., "An Implicit Multigrid Method by Agglomeration Applied to Turbulent Flows," *Computers and Fluids*, Vol. 26, No. 3, 1997, pp. 299–320.

[46]Carré, G., Fournier, L., and Lanteri, S., "Parallel Linear Multigrid Algorithms for the Acceleration of Compressible Flow Calculations," *Computer Methods in Applied Mechanics and Engineering*, Vol. 184, No. 2, 2000, pp. 427–448.

[47]Schumann, U., "Realizability of Reynolds-Stress Turbulence Models," *Physics of Fluids*, Vol. 20, No. 5, 1977, pp. 721–725.

[48]Yokota, J. W., "Diagonally Inverted Lower-Upper Factored Implicit Multigrid Scheme for the 3-D Navier–Stokes Equations," *AIAA Journal*, Vol. 28, No. 9, 1990, pp. 1642–1649.

[49]Edwards, J. R., "Upwind Relaxation Multigrid Method for Computing 3-D Viscous Internal Flows," *Journal of Propulsion and Power*, Vol. 12, No. 1, 1996, pp. 146–154.

[50]Braaten, M. E., and Connell, S. D., "Three-Dimensional Unstructured Adaptive Multigrid Scheme for the Navier–Stokes Equations," *AIAA Journal*, Vol. 34, No. 2, 1996, pp. 281–290.

[51]Gerolymos, G. A., and Vallet, I., "Wall-Normal-Free Near-Wall Reynolds-Stress Closure for Three-Dimensional Compressible Separated Flows," *AIAA Journal*, Vol. 39, No. 10, 2001, pp. 1833–1842.

[52]Gerolymos, G. A., Sauret, E., and Vallet, I., "Contribution to the Single-Point-Closure Reynolds-Stress Modelling of Inhomogeneous Flow," *Theoretical and Computational Fluid Dynamics*, Vol. 17, No. 5–6, 2004, pp. 407–431.

[53]Vallet, I., "Aérodynamique Numérique 3-D Instationnaire avec Fermeture Bas-Reynolds au Second Ordre," Ph.D. Dissertation, Univ. Pierre-et-Marie-Curie, Paris, Dec. 1995.

[54]Gerolymos, G. A., Neubauer, J., Sharma, V. C., and Vallet, I., "Improved Prediction of Turbomachinery Flows Using Near-Wall Reynolds-Stress Model," *Journal of Turbomachinery*, Vol. 124, No. 1, 2002, pp. 86–99.

[55]Settles, G. S., Vas, I. E., and Bogdonoff, S. M., "Details of a Shock-Separated Turbulent Boundary-Layer at a Compression Corner," *AIAA Journal*, Vol. 14, No. 12, 1976, pp. 1709–1715.

[56]Dolling, D. S., and Murphy, M. T., "Unsteadiness of the Separation Shock-Wave Structure in a Supersonic Compression Ramp Flowfield," *AIAA Journal*, Vol. 21, No. 12, 1983, pp. 1628–1634.

[57]Gerolymos, G. A., Tsanga, G., and Vallet, I., "Near-Wall k–ε Computation of Transonic Turbomachinery Flows with Tip Clearance," *AIAA Journal*, Vol. 36, No. 10, 1998, pp. 1769–1777.

[58]Doukelis, A., Mathioudakis, K., and Papailiou, K. D., "Detailed Flow and Overall Performance Measurements for Different Clearance Configurations in the NTUA Annular Cascade Facility," Final Rept., APPACET Project, EEC Contract BRPR-CT97-0610, 2000, Chap. 3.

[59]Doukelis, A., Mathioudakis, K., and Papailiou, K. D., "Hub Wall Rotation Influence on High-Speed Compressor Cascade Performance," *Journal of Propulsion and Power*, Vol. 17, No. 4, 2001, pp. 902–908.

[60]Vinokur, M., "An Analysis of Finite-Difference and Finite-Volume Formulations of Conservation Laws," *Journal of Computational Physics*, Vol. 81, No. 1, 1989, pp. 1–52.

[61]Anderson, W. K., Thomas, J. L., and Van Leer, B., "Comparison of Finite-Volume Flux-Vector-Splittings for the Euler Equations," *AIAA Journal*, Vol. 24, No. 9, 1986, pp. 1453–1460.

[62]Anderson, W. K., Thomas, J. L., and Rumsey, C. L., "Extension and Application of Flux-Vector-Splitting to Calculations on Dynamic Meshes," *AIAA Journal*, Vol. 27, No. 6, 1989, pp. 673,674; also AIAA Paper 87-1152, June 1987.

[63]Arnone, A., "Viscous Analysis of 3-D Rotor Flow Using a Multigrid Method," *Journal of Turbomachinery*, Vol. 116, July 1994, pp. 435–445.

[64]Zhao, Y., "Computation of Complex Turbulent Flow Using Matrix-Free Implicit Dual-Time-Stepping Scheme and LRN Turbulence Model on Unstructured Grids," *Computers and Fluids*, Vol. 33, No. 1, 2004, pp. 119–136.

[65]Chakravarthy, S. R., "Euler Equations—Implicit Schemes and Boundary Conditions," *AIAA Journal*, Vol. 21, No. 5, 1983, pp. 699–706.

[66]Giles, M. B., "Nonreflecting Boundary Conditions for Euler Equation Calculations," *AIAA Journal*, Vol. 28, No. 12, 1990, pp. 2050–2058.

[67]Mottura, L., Vigevano, L., and Zaccanti, M., "Factorized Implicit Upwind Methods Applied to Inviscid Flows at High Mach Number," *AIAA Journal*, Vol. 38, No. 10, 2000, pp. 1846–1852.

[68]MacCormack, R. W., "Iterative Modified Approximate Factorization," *Computers and Fluids*, Vol. 30, 2001, pp. 917–925.

[69]Koren, B., "Defect Correction and Multigrid for an Efficient and Accurate Computation of Airfoil Flows," *Journal of Computational Physics*, Vol. 77, No. 1, 1988, pp. 183–206.

[70]MacCormack, R. W., "A Numerical Method for Solving the Equations of Compressible Viscous Flow," *AIAA Journal*, Vol. 20, No. 9, 1982, pp. 1275–1281.

[71]Leclercq, M. P., and Stoufflet, P. L., "Characteristic Multigrid Method Application to Solve the Euler Equations with Unstructured and Unnested Grids," *Journal of Computational Physics*, Vol. 104, No. 2, 1993, pp. 329–346.

[72]Warming, R. F., Beam, R. M., and Hyett, B. J., "Diagonalization and Simultaneous Symmetrization of the Gas-Dynamic Matrices," *Mathematics of Computation*, Vol. 29, No. 132, Oct. 1975, pp. 53–72.

[73]Radespiel, R., and Swanson, R. C., "Progress with Multigrid Schemes for Hypersonic Flow Problems," *Journal of Computational Physics*, Vol. 116, No. 1, 1995, pp. 103–122.

[74]Piquet, J., *Turbulent Flows—Models and Physics*, Springer-Verlag, Berlin, 1999, pp. 102–132, 273–284.

[75]Gerolymos, G. A., Sauret, E., and Vallet, I., "Oblique-Shock-Wave/Boundary-Layer Interaction Using Near-Wall Reynolds-Stress Models," *AIAA Journal*, Vol. 42, No. 6, 2004, pp. 1089–1100.

[76]Rizzi, A., Eliasson, P., Lindblad, I., Hirsch, C., Lacor, C., and Haeuser, J., "The Engineering of Multi-Block/Multigrid Software for Navier–Stokes Flows on Structured Meshes," *Computers and Fluids*, Vol. 22, No. 2/3, 1993, pp. 341–367.

[77]Gerolymos, G. A., and Tsanga, G., "Biharmonic 3-D Grid Generation for Axial Turbomachinery with Tip-Clearance," *Journal of Propulsion and Power*, Vol. 15, No. 3, 1999, pp. 476–479.

R. So
Associate Editor

Color reproductions courtesy of Université Pierre-et-Marie-Curie.